Downloaded from rsta.royalsocietypublishing.org

PHILOSOPHICAL TRANSACTIONS OF THE ROYAL SOCIETY A
MATHEMATICAL, PHYSICAL & ENGINEERING SCIENCES

Chemical Analyses and Studies of Electronic Structure of Solids by Electron Energy Loss Spectroscopy with an Electron Microscope [and Discussion]

J. M. Thomas, T. G. Sparrow, M. K. Uppal, B. G. Williams and D. Norman

Phil. Trans. R. Soc. Lond. A 1986 **318**, 259-281
doi: 10.1098/rsta.1986.0075

Email alerting service Receive free email alerts when new articles cite this article - sign up in the box at the top right-hand corner of the article or click here

To subscribe to *Phil. Trans. R. Soc. Lond. A* go to: http://rsta.royalsocietypublishing.org/subscriptions

This journal is © 1986 The Royal Society

Downloaded from rsta.royalsocietypublishing.org

Phil. Trans. R. Soc. Lond. A **318**, 259–281 (1986) [259]
Printed in Great Britain

Chemical analyses and studies of electronic structure of solids by electron energy loss spectroscopy with an electron microscope

By J. M. Thomas, F.R.S., T. G. Sparrow, M. K. Uppal and B. G. Williams
Department of Physical Chemistry, University of Cambridge, Lensfield Road, Cambridge CB2 1EP, U.K.

[Plates 1 and 2]

Both the thickness and the composition of a specimen can be deduced from plasmon spectroscopy, which is readily recorded with an electron microscope to which has been attached an electron spectrometer of resolution 1–3 eV. This is illustrated in the study of alkali metals and sp metals such as magnesium and aluminium, which are produced by decomposing ternary or binary hydrides (for example, $NaAlH_4$ or MgH_2). But other materials, including silicon, are also amenable to studies of this kind.

The elemental composition, electronic structure and inter-atomic distances of a sample can be derived from the core-electron (K, L, M edge) loss peaks and their fine structure. And from the near-edge energy loss structure, and in particular from the 'white line' intensity ratios (for example, L_2/L_3), the number of d-electrons and hence the oxidation state of transition elements in compounds of first-row transition-metal series may be determined.

In the region beyond the near-edge structure, extended electron energy loss fine structure (e.x.e.l.f.s.) is observed and this may be used to obtain information about the local co-ordination of different atoms in the sample.

Finally, by monitoring the Doppler broadening of the scattered electrons liberated from the sample as a consequence of the 'electron' equivalent of the Compton process, we can probe the electronic properties of the solid in momentum space. This reveals the nature of the bonding in simple solids; and, in particular, reveals whether an amorphous sample of carbon is more nearly graphitic or adamantine.

1. Introduction

High-resolution electron microscopy (h.r.e.m.) is a powerful analytical tool for the study of solids, especially those possessing high areas. Among other things, it permits the identification of crystallographic phases by electron diffraction; it yields, in real space, the projected view of the atomic structure of the material under investigation at the sub-nanometre level; and it enables us to arrive at the stoichiometry or composition from the electron-induced, X-ray emission spectrum. To interpret high-resolution images it is necessary to model the process of image formation in the microscope, but programs to do this are available (Goodman & Moodie 1974; Jefferson *et al.* 1976), and then, provided there is local order and we have some idea as to what the structure ought to be, we can, from the high-resolution image, 'read off' the location of the various atomic constituents. When we do not know the structures or the composition of the materials under investigation, high-resolution electron microscopy is complemented, in a vital fashion, by electron energy loss spectroscopy. Although the energy resolution is very much poorer, the spatial resolution is very much better than that used to study adsorbates at solid surfaces with low-energy electron loss spectroscopy of the kind

The Royal Society is collaborating with JSTOR to digitize, preserve, and extend access to *Philosophical Transactions of the Royal Society of London. Series A, Mathematical and Physical Sciences.* www.jstor.org

Downloaded from rsta.royalsocietypublishing.org

discussed by Ibach and Sheppard in this symposium, or by using inelastic loss tunnelling spectroscopy (Weinberg 1978).

In this paper we discuss the various electron energy loss processes that can be observed in an electron microscope and illustrate some of the ways in which e.e.l.s. can be used to obtain information relating to the chemistry and electronic properties of our samples.

2. Apparatus

Figure 1 shows a schematic diagram of a transmission electron microscope to which a spectrometer has been attached. The electrons emitted by the filament are accelerated to an energy that is usually between 100 and 200 keV; the condenser lenses collect the electrons and focus them onto the sample. The electrons that pass through the sample are focused by the objective lens to produce a magnified image or diffraction pattern of the sample. The next set

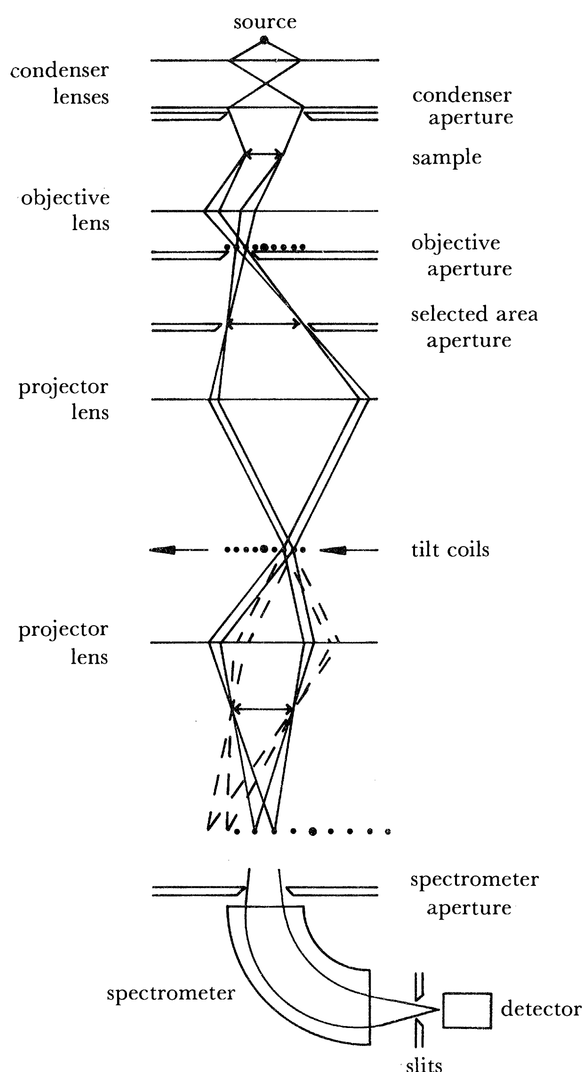

Figure 1. Schematic diagram of electron microscope and spectrometer. Ray paths are indicated for a Compton scattering experiment. Double-headed arrows indicate image planes; dots indicate diffraction planes.

PHILOSOPHICAL TRANSACTIONS OF THE ROYAL SOCIETY A MATHEMATICAL, PHYSICAL & ENGINEERING SCIENCES
PHILOSOPHICAL TRANSACTIONS OF THE ROYAL SOCIETY A MATHEMATICAL, PHYSICAL & ENGINEERING SCIENCES

Downloaded from rsta.royalsocietypublishing.org

of lenses project this image or diffraction pattern onto the viewing screen, immediately below which is a magnetic prism spectrometer, in which the electron beam is deflected through 90° and the electrons are dispersed according to their energies. By scanning these electrons over a slit and using a scintillator coupled to a photomultiplier, an energy loss spectrum can be obtained with a resolution of between 1 and 4 eV. In addition to all of this, there are a number of apertures down the length of the microscope so that it is possible to limit the divergences of the various beams or alternatively to select only those electrons that enter or leave the sample at a well defined angle.

2.1. *Outline of principles used in e.e.l.s.*

With the aid of such a microscope we are able to study a variety of energy loss processes, as illustrated schematically in figure 2. The range of energies over which we obtain reasonable signals extends to about 2000 eV below the incident energy. The zero-loss peak, at the energy

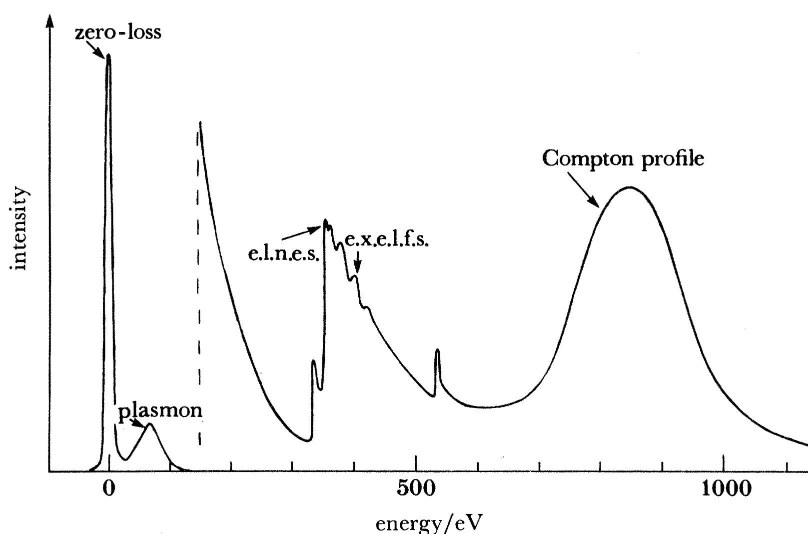

FIGURE 2. Schematic diagram of the possible energy loss processes that can be observed in an electron microscope.

of the incident beam, arises partly from those electrons that are scattered elastically in the forward direction, but since the resolution is not sufficient to resolve phonon energies, which are typically of the order of one tenth of an electronvolt or less, this also includes thermal diffuse scattering. Proceeding through progressively increasing loss of energy, the first feature of interest is the plasmon peak, and this usually occurs between about 5 and 25 eV. Since plasmons are collective excitations of the electron gas their energies are governed by the density of the electrons in the sample and the extent to which the electrons are free or bound: clearly it is much easier to excite a collective oscillation if the electrons in the sample are free.

At higher energy losses the intensity falls by several orders of magnitude but, if the vertical scale is changed, steps are observed at energies corresponding to the binding energies of the electrons in the sample. These occur at all energies from a few electronvolts to hundreds of thousands of electronvolts, but since these experiments cover a loss range of about 2 keV, the observed binding energies correspond to the outer 2 or 3 shells of electrons. The point here is

Downloaded from rsta.royalsocietypublishing.org

MATHEMATICAL, PHYSICAL & ENGINEERING SCIENCES
THE ROYAL SOCIETY A
PHILOSOPHICAL TRANSACTIONS OF

that an electron will be excited only when the energy transfer is greater than the binding energy, but that, once this point is reached, there will be an abrupt increase in the scattering cross section. Since the height of the step is proportional to the amount of that element that is present, the edges can be used to determine the chemical composition of the sample, if the cross section for exciting that edge is known.

A closer examination of the edge shows that it is not just a simple step, but that there is significant fine structure. This structure reflects the energy density of unoccupied states in the region of the Fermi energy and provides information relating to the band structure; but it also depends on the core hole that is left behind when an electron is ejected from its ground state, so that excitonic effects must be included in a full description.

Beyond this near-edge structure there is further structure, which is essentially the electron equivalent of X-ray absorption fine structure or e.X.a.f.s., and goes under the abbreviation of e.x.e.l.f.s. for extended energy loss fine structure. This arises from interference effects due to neighbouring atoms when one tries to eject electrons from a particular atom with a wavelength of the order of the nearest-neighbour distance, and therefore yields information about the local coordination of the atom whose edge is under investigation.

Finally, if in addition to all of this, one looks not at the electrons that have been transmitted straight through the sample, but at electrons that have been scattered through an angle of about 5°, one finds the Compton profile. As we shall see, the Compton profile provides a measure of the ground-state momentum wavefunction of the electrons in the sample.

3. Plasmon scattering

The concept of plasmons as collective excitations of a gas of ionized particles derives from the study of gaseous discharges by Tonks & Langmuir (1929). By using simple classical arguments they obtained the well known expression for the frequency of the plasma oscillations in terms of the electron density

$$\omega = (ne^2/m\epsilon)^{\frac{1}{2}}. \tag{3.1}$$

The first use of the plasmon concept in the study of metals seems to have been by Kronig, Korringa and Kramers (Kronig & Korringa 1943; Kramers 1947; Kronig 1949). Subsequently, Ruthemann, Bohm, Pines and others extended this work and developed the full quantum-mechanical theory of plasmons (Ruthemann 1948; Lang 1948; Bohm & Gross 1949*a*; Bohm & Gross 1949*b*; Bohm and Pines 1951, 1953; Pines & Bohm 1952; Pines 1953).

For the free-electron metals, the conduction electrons may be treated as a Fermi gas, so that the plasmon concept applies quite precisely. One may then derive the expression for the plasma frequency simply by imagining that the sea of electrons is displaced sideways and then released. The restoring force is linear, the oscillation is simple harmonic and the frequency is given by (3.1). Figure 3 shows a collection of plasmon spectra, which we have measured for various free-electron metals, and in each case the plasmon lines are well defined. Indeed, successive excitations of plasmons produce whole families of lines, each at an integral multiple of the fundamental plasmon energy. A plot of the measured plasmon energies against the values calculated from the simple free-electron formula (figure 4) yields excellent agreement between the two. Plasmon spectra are therefore seen to provide a rapid means of identifying these elements in their metallic state.

Downloaded from rsta.royalsocietypublishing.org

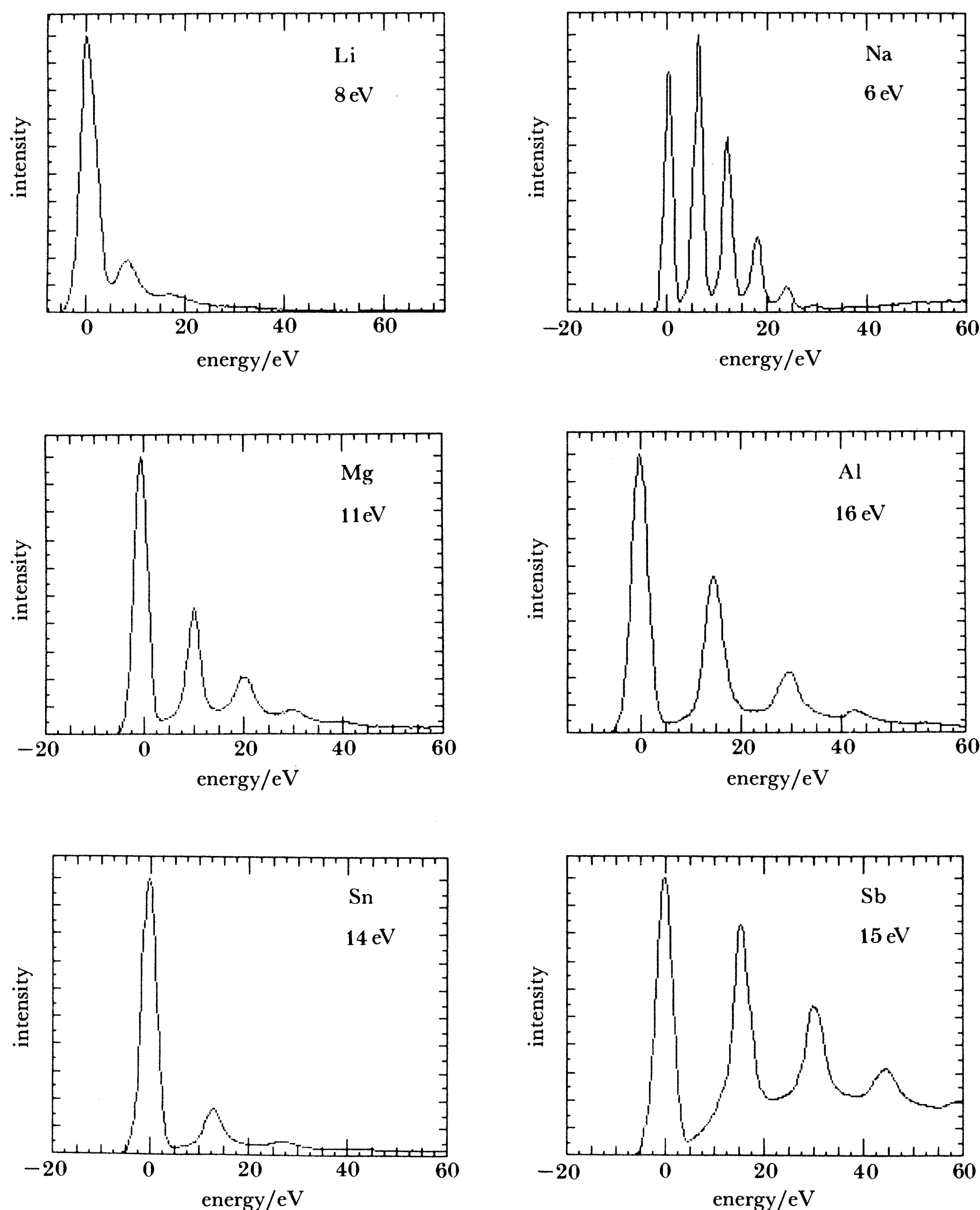

FIGURE 3. Plasmon spectra for various free-electron metals.

This can be illustrated by using measurements on samples that were nominally magnesium hydride (Sparrow *et al.* 1983). Such hydrides are of much interest as vehicles for the storage of hydrogen. Our interest in these samples arose from the fact that in addition to the bulk material, long, straight whiskers were present, as can be seen in figure 5*a*, plate 1. The whiskers are typically 10 μm long and 0.1 μm across, and the problem was to determine their composition. The plasmon spectrum from the bulk material shown in figure 6 was much broader than those we saw for the free-electron metals and this is indeed typical of the plasmon spectra for

Downloaded from rsta.royalsocietypublishing.org

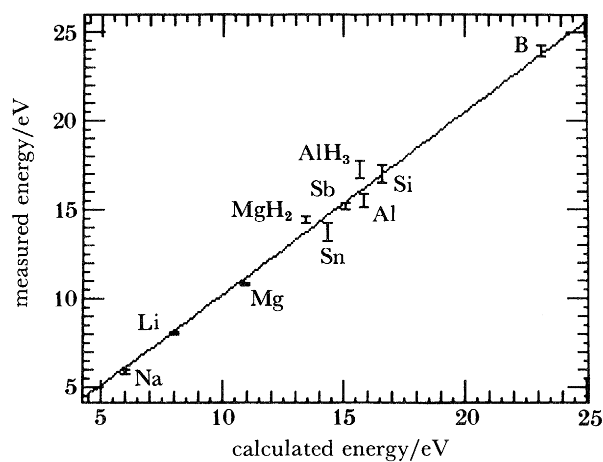

FIGURE 4. Plot of measured plasmon energies against values calculated from the free-electron model (equation (3.1)).

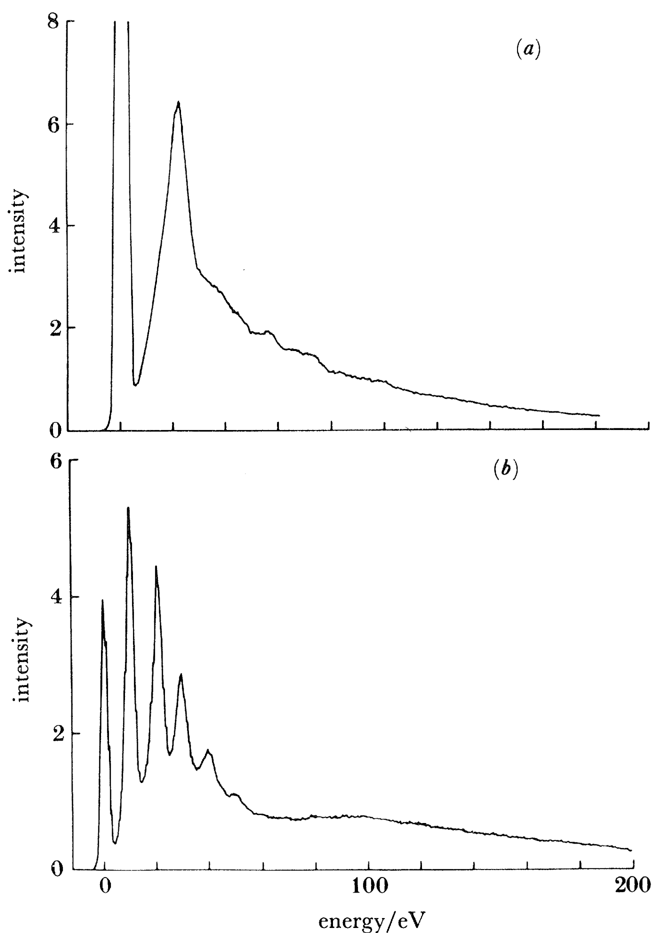

FIGURE 6. (*a*) Plasmon spectrum of MgO from the bulk. (*b*) Plasmon spectrum of magnesium metal from the whisker.

PHILOSOPHICAL TRANSACTIONS OF THE ROYAL SOCIETY A MATHEMATICAL, PHYSICAL & ENGINEERING SCIENCES

PHILOSOPHICAL TRANSACTIONS OF THE ROYAL SOCIETY A MATHEMATICAL, PHYSICAL & ENGINEERING SCIENCES

Downloaded from rsta.royalsocietypublishing.org

FIGURE 5. (*a*) Magnesium whisker on holey carbon film. (*b*) Tip of whisker where aluminium is present. (*c*) E.d.a.X. spectra of whisker from regions progressively closer to tip.

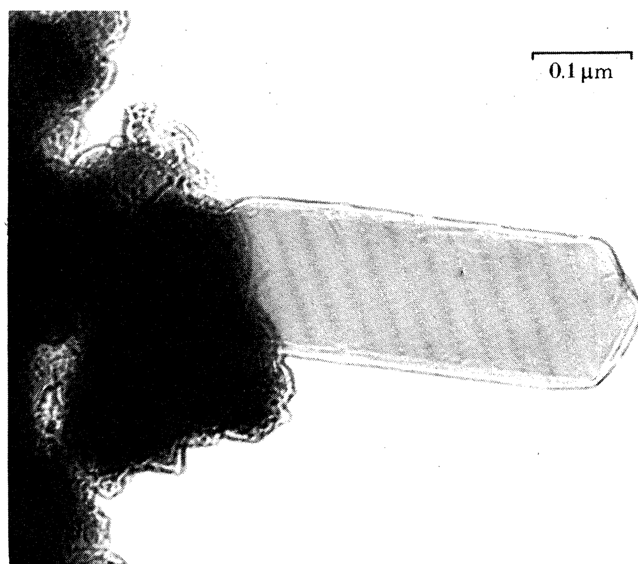

FIGURE 8. Sodium crystal grown out from $NaAlH_4$ sample, as a result of exposure to the electron beam.

(*Facing p.* 264)

Downloaded from rsta.royalsocietypublishing.org

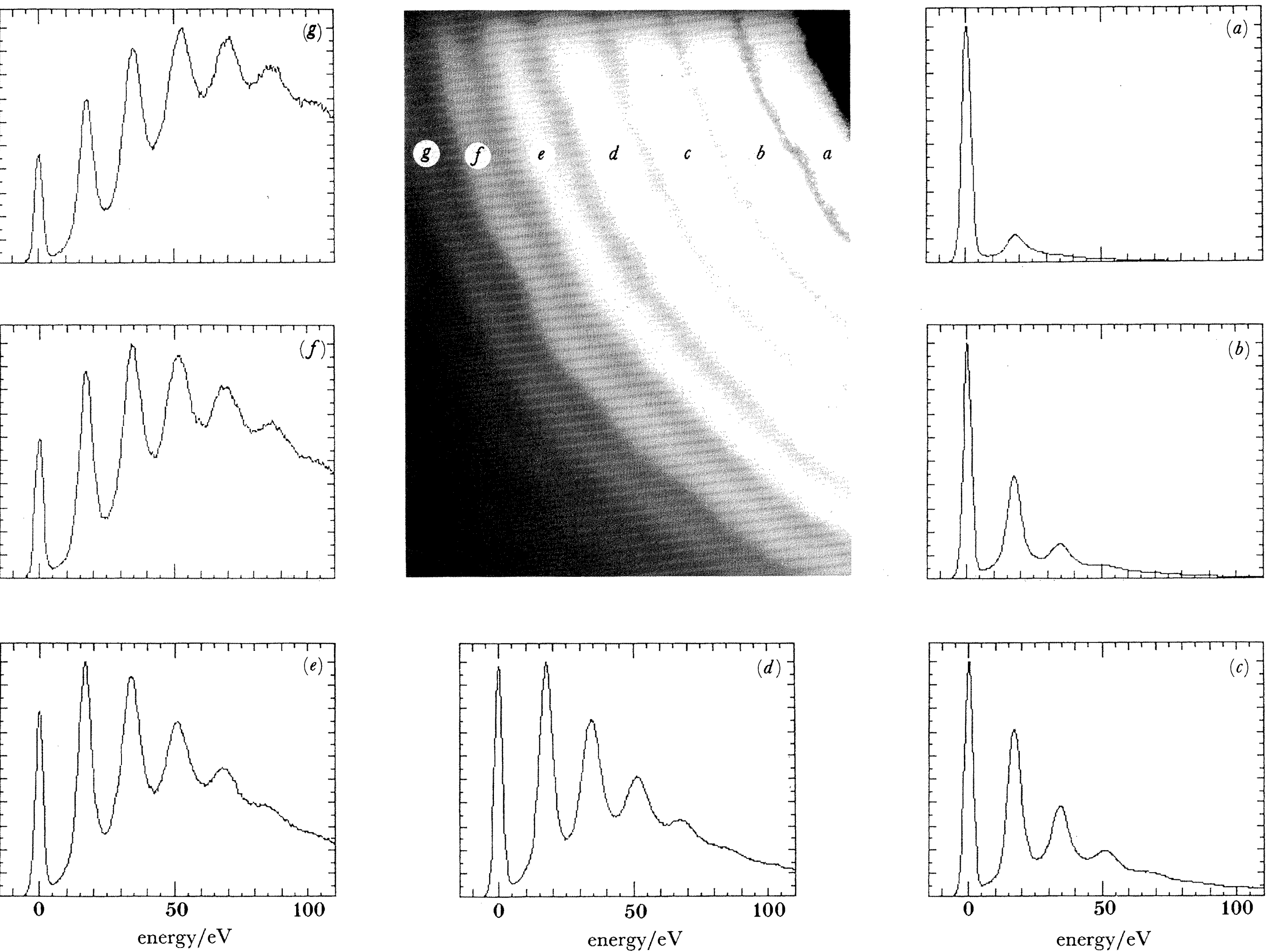

FIGURE 10. Thickness fringes in a single crystal of silicon. There is a hole at the top right corner and the thickness increases towards the bottom left. Plasmon spectra measured at each successive fringe as indicated. Each fringe corresponds to an increase in thickness of about 600 Å.

Downloaded from rsta.royalsocietypublishing.org

insulators. Furthermore, it did not degrade even after prolonged exposure to the electron beam and an oxygen edge was found in the loss spectrum: we concluded, therefore, that the bulk material was magnesium oxide. However, the plasmon spectrum of the whiskers (figure 6) is unmistakably that of pure magnesium metal, so that we were able to identify the whiskers, rapidly and unequivocally. We could go even further; at the tip of most of the whiskers was a tiny speck of some other material (figure 5*b*), and their plasmon spectra (figure 7) showed

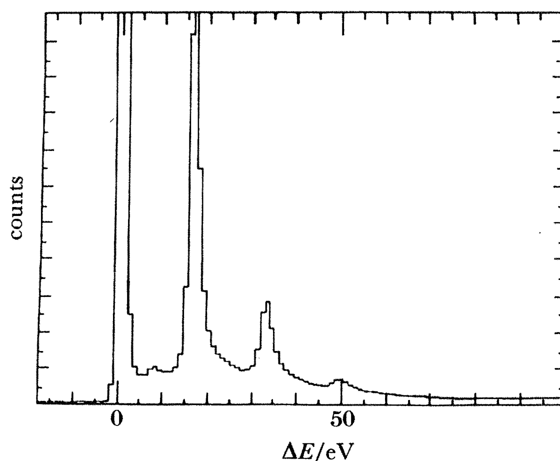

FIGURE 7. Plasmon spectrum of aluminium metal from the tip of the whisker.

them to be pure aluminium. This led us to conclude that, when the material was prepared, very small amounts of aluminium in the starting material had formed a low-melting-point eutectic with the magnesium, and that this served to catalyse the growth of the whiskers. Subsequently, energy-dispersive X-ray (e.d.a.X.) emission measurements from the needles and the tip confirmed this observation (figure 5*c*).

Another instance in which the plasmon spectroscopy proved crucial was in the decomposition of sodium aluminium hydride, $NaAlH_4$ (Jones *et al.* 1984) induced by an electron beam. It is well known that when certain metal hydrides are irradiated with photons or electrons they decompose with the evolution of hydrogen: indeed $LiAlH_4$ is nowadays used (Boldyrev 1985, personal communication) in non-silver photography. In the electron microscope it was observed that, as the starting material degrades, small filamentary growths of a crystalline nature appear, as can be seen from the faceted nature of their growth (figure 8). Although these growths are very short-lived in the electron beam, and disappear after only a few seconds, we were again able to show from their plasmon spectra (figure 9) that they are crystals of pure metallic sodium.

Plasmon spectra also provide a ready means of measuring the thickness of films in the electron microscope. To illustrate this we have used a single crystal of silicon, which as been thinned in such a way as to produce a wedge-shaped edge, so that in figure 10, plate 2, there is a hole in the top right corner and the crystal gets thicker towards the bottom left; the thickness fringes then gave us one measure of the sample thickness and we measured the plasmon spectrum at each successive fringe as indicated in the figure. Each fringe corresponds to an increase in the thickness of approximately 60 nm and when the number of the fringe is plotted against the

Downloaded from rsta.royalsocietypublishing.org

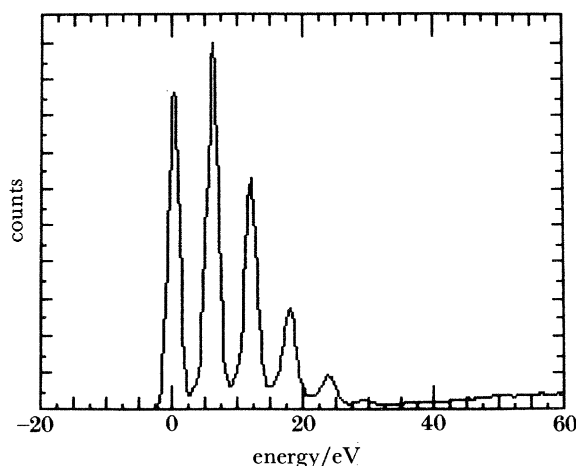

FIGURE 9. Plasmon spectrum of sodium metal from the crystal shown in figure 8.

logarithm of the ratio of the total intensity to the intensity in the zero-loss peak as in figure 11, an excellent linear relation results. Plasmon spectra can therefore serve as a convenient means of measuring relative thicknesses down to a few nanometres with an accuracy of about 5% and, provided the measurements can be calibrated by using thickness fringes, or some other means, absolute thicknesses can be determined with the same precision.

So far we have considered only bulk plasmons, but it is also possible to excite surface plasmons (Raether 1980). For these, the plasmon frequency, and therefore energy, depends on the geometry of the surface, but for a two-dimensional plane surface it is not difficult to show that the plasmon frequency is reduced by a factor of $2^{\frac{1}{2}}$. Figure 12 shows surface plasmons measured from small particles of Al and Sb and they do indeed occur at an energy that is $2^{\frac{1}{2}}$ less than that of their bulk plasmons. Another potentially useful aspect of surface plasmons follows from the observation that the ϵ in the expression for the plasma frequency refers to the dielectric constant of the medium surrounding the sample, so that surface plasmons are sensitive to

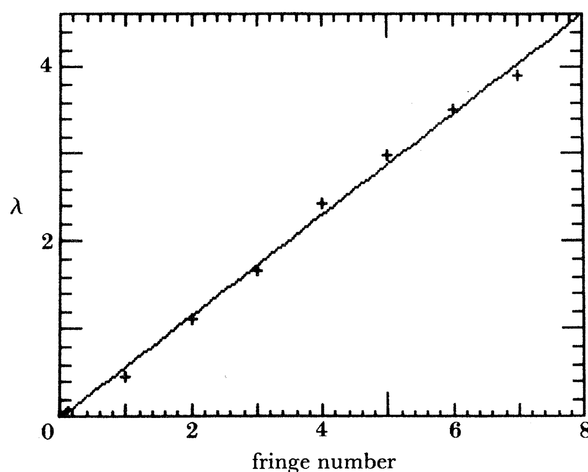

FIGURE 11. Plot of fringe number against λ, the logarithm of the ratio of the total intensity to the intensity in the zero-loss peak for each spectrum in figure 10. The slope of the graph is 0.577 ± 0.009.

PHILOSOPHICAL TRANSACTIONS OF THE ROYAL SOCIETY A MATHEMATICAL, PHYSICAL & ENGINEERING SCIENCES

PHILOSOPHICAL TRANSACTIONS OF THE ROYAL SOCIETY A MATHEMATICAL, PHYSICAL & ENGINEERING SCIENCES

Downloaded from rsta.royalsocietypublishing.org

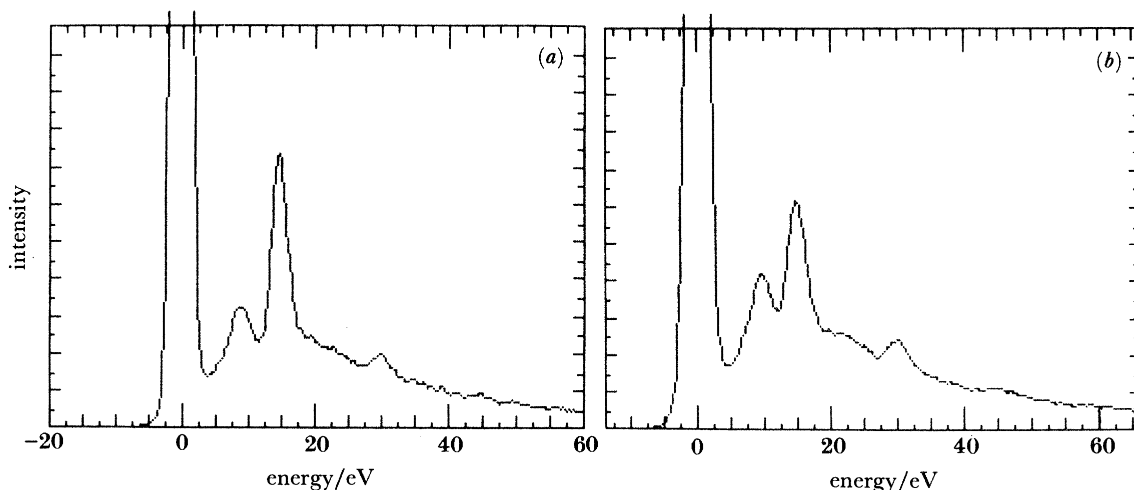

FIGURE 12. Surface and bulk plasmons from (*a*) aluminium and (*b*) antimony. The surface plasmons occur at an energy corresponding to the energy of the bulk plasmons divided by $2^{\frac{1}{2}}$.

contamination or to surface layers in general. Krane & Raether (1976) have observed two surface plasmons in thin films of aluminium deposited on carbon; one at an energy of 10.2 eV from the aluminium–vacuum interface and the other at 7.4 eV from the aluminium–carbon interface.

4. Chemical analysis

The next most prominent feature in our schematic energy loss spectrum (figure 1) is the edge at an energy transfer corresponding to the binding energy of the core electrons in the sample. We illustrate this with data for MnO_2 and Fe_2O_3 shown in figure 13 and the oxygen K-edge at 532 eV as well as the manganese and iron edges, at 640 eV and 708 eV respectively, are clearly evident. If we subtract a suitable background, measure the intensity under the edge over a suitable energy range and then calculate the cross section for exciting each edge, under

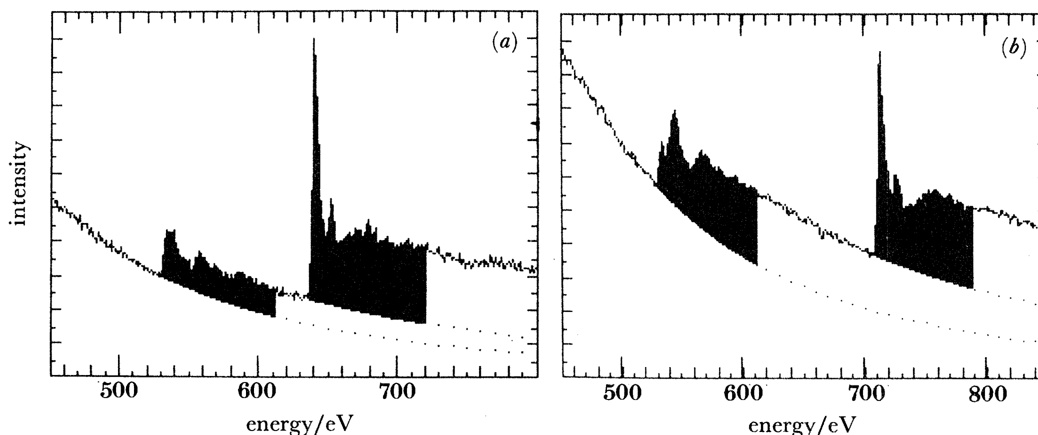

FIGURE 13. E.e.l.s. of (*a*) MnO and (*b*) Fe_2O_3. Power-law backgrounds have been fitted as indicated by the dotted lines. The shaded areas are 80 eV windows above each edge used in the determination of the chemical composition as described in the text.

PHILOSOPHICAL TRANSACTIONS OF THE ROYAL SOCIETY A MATHEMATICAL, PHYSICAL & ENGINEERING SCIENCES

PHILOSOPHICAL TRANSACTIONS OF THE ROYAL SOCIETY A MATHEMATICAL, PHYSICAL & ENGINEERING SCIENCES

Downloaded from rsta.royalsocietypublishing.org

the appropriate experimental conditions (Egerton 1978, 1979, 1981 *a–c*, 1982) we can easily estimate how much of each element is present. As a rough rule of thumb, one can generally make a quantitative elemental analysis with an accuracy of about 10% and the detection limit is also about 10%, but these numbers do vary greatly, depending on the element one is looking for, as well as on the other elements that are present. To illustrate this, table 1 shows the results of making chemical analyses in this way on a variety of samples and the ratios from the assumed compositions are seen to be in good agreement with those obtained by using e.e.l.s.

Under favourable conditions some quite striking results can be obtained, and an interesting example of this is in the detection of nitrogen in platelets in diamond shown in figure 14 (Bursill

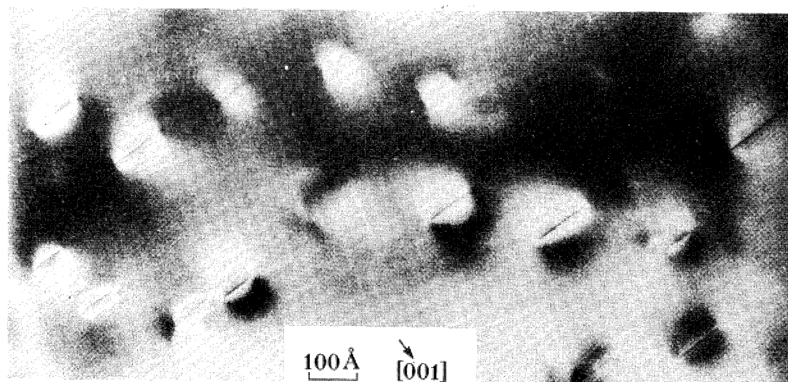

FIGURE 14. Electron micrograph showing small (100–200 Å diameter) (001) platelets in [100] projection of type 1A diamond. Dark lines indicate edge-on platelets, which are surrounded by black and white strain contrast (Bursill *et al.* 1981). (1 Å = 10^{-1} nm = 10^{-10} m.)

TABLE 1. COMPARISON OF RATIOS FROM ASSUMED COMPOSITIONS WITH THOSE OBTAINED FROM E.E.L.S.

sample	ratio by chemical formula	ratio by experiment
boron nitride	B:N = 1.0	0.91
manganese dioxide	O:Mn = 2.0	2.07
ferric oxide	O:Fe = 1.5	1.48
rhodizite	B:O = 0.404	0.39
	O:Be = 6.211	6.67
clay	F:Mg = 0.25 to 0.4	0.39
	F:Si = 0.22 to 0.4	0.29

et al. 1981). Although these platelets were first observed directly with transmission electron microscopy as early as 1962 (Evans & Phaal 1962), their structure and composition remained a puzzle until very recently. In particular, the various models that had been proposed assumed that nitrogen played an important role in the formation of these platelets. Using e.e.l.s., Berger & Pennycook (1982) were able to show clearly that nitrogen was present in the platelets, as can be seen from the e.e.l.s. spectra shown in figure 15. These experiments were not easy to do. The platelets themselves are small and the amount of nitrogen present is still smaller; but repeated measurements under very carefully controlled conditions show that nitrogen is indeed concentrated in the regions of the platelets.

Downloaded from rsta.royalsocietypublishing.org

PHILOSOPHICAL TRANSACTIONS OF THE ROYAL SOCIETY A MATHEMATICAL, PHYSICAL & ENGINEERING SCIENCES

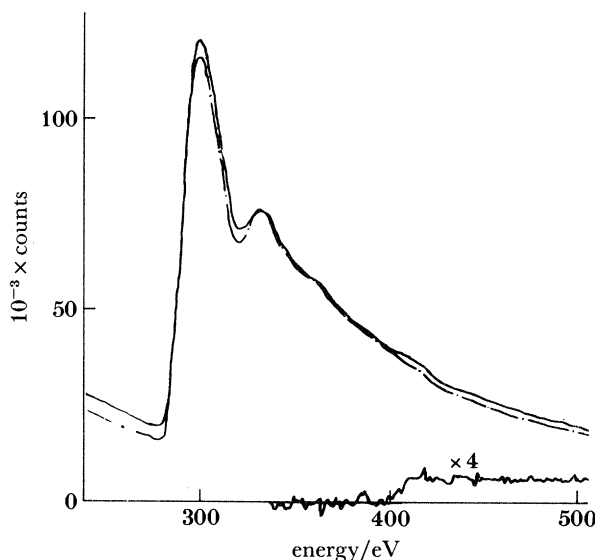

FIGURE 15. Electron energy loss spectra from the centre of a platelet (solid line) and from just off the platelet (chained line). Also shown is the difference (×4), which shows the nitrogen K edge from the platelet, at approximately 406 eV (Bursill *et al.* 1981).

5. Electron loss near-edge structure

It is clear that there is a certain amount of structure associated with the edges and if we fit, and then subtract, a suitable background this structure stands out more clearly (figure 16). This energy loss near-edge structure, or e.l.n.e.s. is the electron scattering counterpart of X-ray absorption near-edge structure (X.a.n.e.s.). Its occurrence arises, at least in part, from the energy density of unoccupied states. Clearly, a particular transition can take place only if there is an empty state available to accommodate the excited electron, but the structure also depends on the initial state, through the dipole selection rules, and on the interaction between the excited state and the core hole that remains, so that it is necessary to include excitonic effects in a full description. We can, however, make some progress in understanding the structure of these edges by using fairly simple arguments. As illustrated schematically in figure 17, the transition-metal d-bands are rather narrow, having a width of only a few electronvolts. Any transition from a core level to the d-band will therefore have a reasonably well defined energy, and this is why sharp lines are observed at transition-metal L edges. In addition to this, the L level is split, with the $2p_{\frac{1}{2}}$ and $2p_{\frac{3}{2}}$ levels having different energies so that there are two lines at the edge.

We might expect the intensities of these lines, relative to the shoulder that arises from transitions to the continuum, to increase as the number of empty d-states increases. This is indeed what we find as we go from MnO with five d-electrons in the d-subshell, to MnO_2 with three and then to $KMnO_4$ with none (figure 16). The intensities of these lines may therefore be used to estimate the number of d-electrons and hence the oxidation state of elements in compounds of the first-row transition-metal series.

The second prediction we might make is that the ratio of the intensities of these two lines should reflect the degeneracy of the initial energy levels so that the L_3 line should be twice as intense as the L_2 line. Now the L_3 line is certainly more intense than the L_2 line, but the ratio is not, in general, two. This is illustrated in figure 18 for a series of transition-metal sesqui-oxides

Downloaded from rsta.royalsocietypublishing.org

PHILOSOPHICAL TRANSACTIONS OF THE ROYAL SOCIETY A MATHEMATICAL, PHYSICAL & ENGINEERING SCIENCES

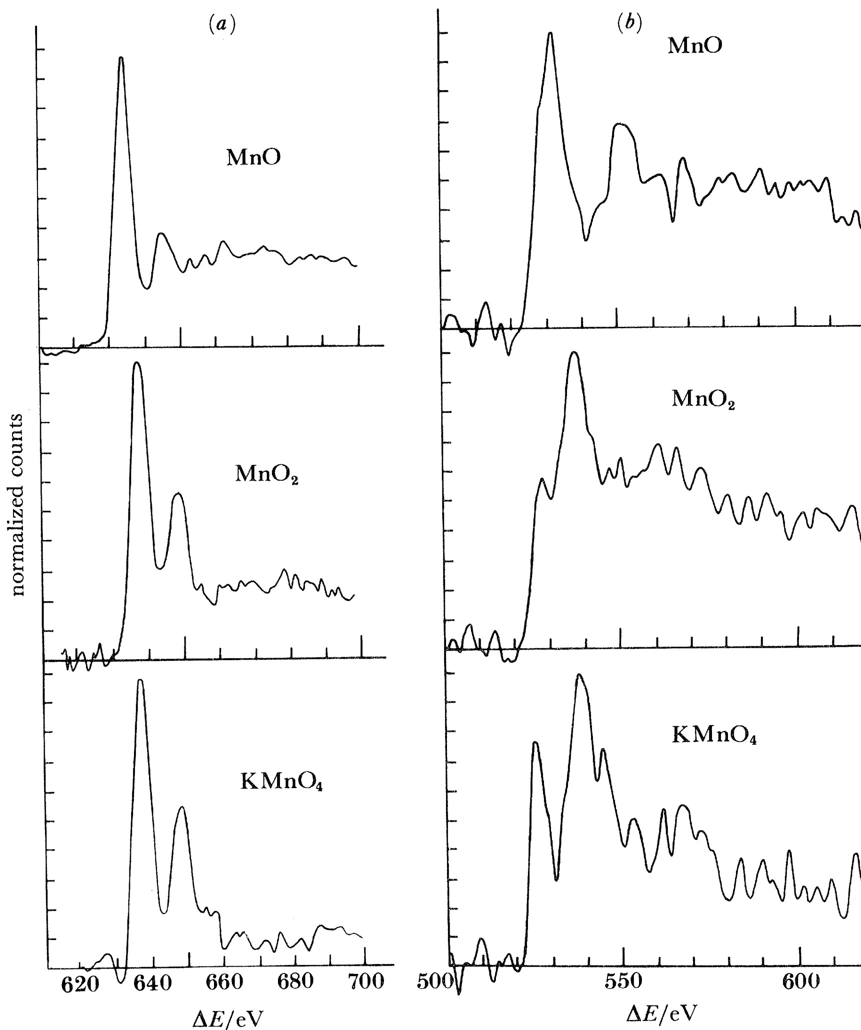

FIGURE 16. Near-edge structure in MnO, MnO_2 and $KMnO_4$. (*a*) Manganese L edges showing the L_2 and L_3 lines. (*b*) Oxygen K edges showing the emergence of a pre-edge peak in $KMnO_4$.

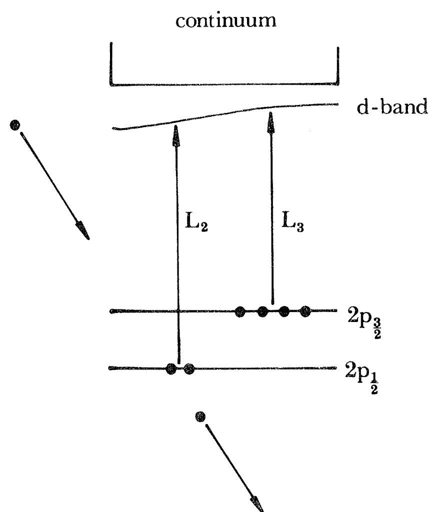

FIGURE 17. Schematic diagram of the band structure of a 3d transition metal, indicating the origin of the L_2 and L_3 lines as a result of the scattering process.

PHILOSOPHICAL TRANSACTIONS OF THE ROYAL SOCIETY A MATHEMATICAL, PHYSICAL & ENGINEERING SCIENCES

Downloaded from rsta.royalsocietypublishing.org

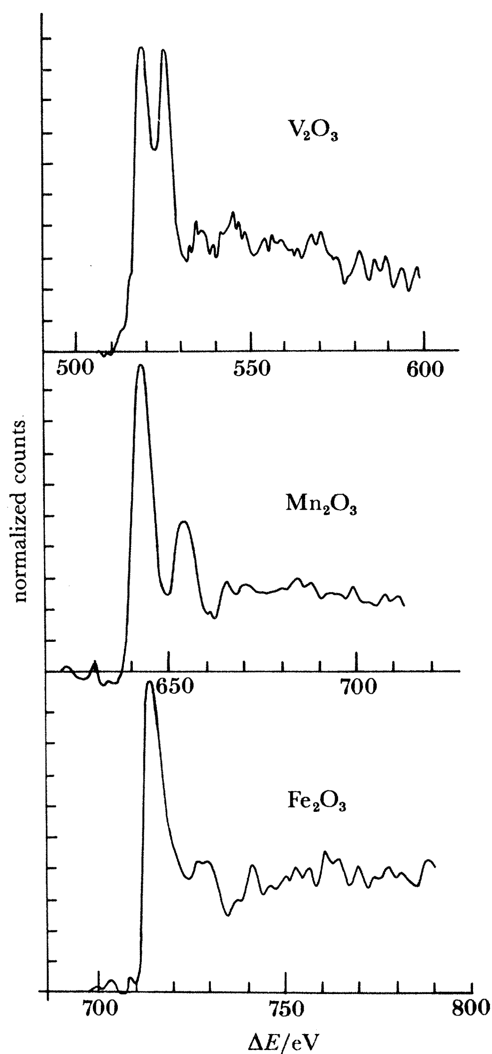

FIGURE 18. Near-edge structure in L edges of transition metal sesqui-oxides V_2O_4, Mn_2O_3 and Fe_2O_3.

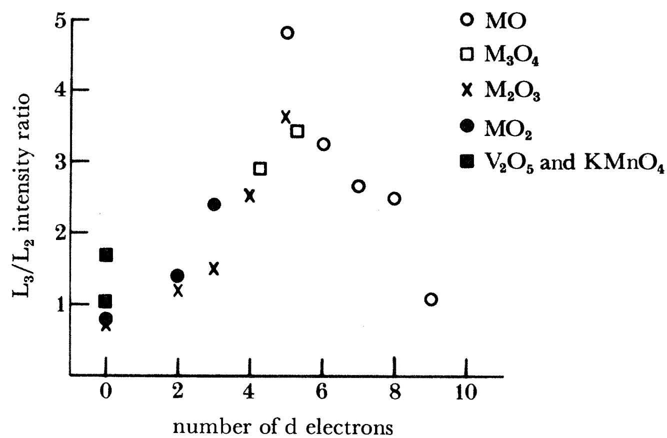

FIGURE 19. Ratio of the intensities of the L_3 and L_2 lines in 3d transition metal oxides plotted against the number of d-electrons.

PHILOSOPHICAL TRANSACTIONS OF THE ROYAL SOCIETY A MATHEMATICAL, PHYSICAL & ENGINEERING SCIENCES

PHILOSOPHICAL TRANSACTIONS OF THE ROYAL SOCIETY A MATHEMATICAL, PHYSICAL & ENGINEERING SCIENCES

Downloaded from rsta.royalsocietypublishing.org

for which the ratio clearly departs significantly from 2. To investigate this further, we measured a large number of transition metal oxides (Rao *et al.* 1984; Thomas *et al.* 1984), and plotted the ratio of the intensities in the two lines against the number of d-electrons (figure 19). As can be seen, this reaches a maximum at $n = 5$ in d^n and this can be explained in terms of the spins of the initial states and the filling of the d-band, first by spin-up electrons and only then by spin-down electrons (Sparrow *et al.* 1984). But the point we want to make here is simply that the L_3/L_2 ratio provides another probe of the oxidation state of the metal.

6. E.x.e.l.f.s.

In the region beyond the near-edge structure, we find further structure, called extended electron energy loss fine structure. These effects are not easy to record (Stephens & Brown 1981; Thomas 1982, 1983) and relatively little work has been done in this area so far; but it can be done and will, we believe, become an important technique in the near future.

The basic idea behind e.x.e.l.f.s. is just the same as in e.X.a.f.s. The effect is observed when the energy transfer is a little greater than the binding energy of the electrons under consideration. As the ejected electron tries to escape from its parent atom it is scattered by the neighbouring atoms (figure 20) and there will be a tendency for the ejected electron to be

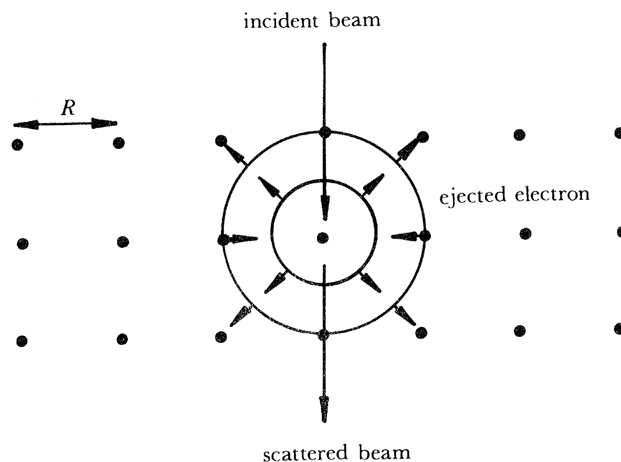

FIGURE 20. Schematic diagram of the e.x.e.l.f.s. scattering process. The ejected electron is scattered back from the surrounding atoms and the interference modulates the observed spectrum.

reflected back from whence it came. Depending on the wavelength of the electron and the distance to the nearest neighbour atoms, the reflected wave will interfere destructively or constructively with that of the ejected electron. If this interference is destructive the probability of such an event occurring will be diminished, and if it is constructive it will be enhanced. The effect will be weak but we expect the probability of any energy loss occurring to be modulated sinusoidally by a term of the form

$$\chi = N \exp(2\pi 2R/\lambda), \tag{6.1}$$

Downloaded from rsta.royalsocietypublishing.org

where λ is the wavelength of the ejected electron and R is the nearest-neighbour distance. The factor of 2 is there because the electron must go to the nearest neighbour and back. Since $2R$ must be about 4 or 5 Å, the electron energy must be about 50 eV or more, so that we should look at the region extending a few hundred volts beyond the edge.

In real life the situation is rather more complicated: when the electron is reflected back there will be a phase change, so this must be added to the exponent; since the strength of the modulation will depend on the number of nearest-neighbour atoms the exponential term is multiplied by N, the number of atoms in the nearest neighbour shell; then, since the ejected electrons spread out as they leave the parent atom the expression must be divided by r^2; because the lattice is not perfectly regular, either because of thermal vibrations or because the sample is amorphous, a damping term must be added depending on the mean square displacement of the atoms. Finally, since the same thing applies to the second shell of neighbours, the third shell, and so on, the whole expression must be repeated and summed over each shell, and so on, so that one finally arrives at the standard expression for e.X.a.f.s. or e.x.e.l.f.s. But the crucial aspect of this is contained in (6.1), namely that the energy loss spectrum should show oscillations beyond the near-edge structure, the wavelengths of which can be related to the distance between the atoms, and the amplitudes of which can be related to the number of atoms in each coordination shell just as with e.X.a.f.s. in X-ray absorption.

Bourdillon *et al.* (1984) have recently reported the results of e.x.e.l.f.s. experiments on amorphous alumina. They had previously studied this system using e.X.a.f.s. so that it provided an ideal test of the viability of e.x.e.l.f.s. For these experiments they prepared samples of amorphous alumina formed on pure aluminium and anodized in a neutral sodium tartrate electrolyte. For comparison, and to confirm the calculated values of the phase shifts, they also studied a specimen of α-alumina thinned by ion bombardment. Finally, they were able to recrystallize the amorphous alumina in the electron beam, to form γ-alumina (confirmed by electron diffraction). Their samples were all about 300 Å thick and this is crucial since the quality of e.x.e.l.f.s. spectra depends on the films being thin enough to minimize the multiple scattering of the electrons.

In e.x.e.l.f.s. it is the low-energy edges that are of interest, since we can most easily measure edges for which the energy is less than about 2 keV. The authors of this work therefore chose the oxygen K edge that occurs at *ca.* 532 eV.

The e.x.e.l.f.s. oscillations are very small and so, as in e.X.a.f.s., one fits a straight line on a log plot to the region above the edge, which is then subtracted, the result of this background subtraction being shown in figure 21. The oscillations are clearly evident, the three sets of data being for α-alumina, amorphous alumina and recrystallized amorphous alumina. To determine the amplitudes and the phases of the oscillations that go to make up this data one simply takes the Fourier transform, which will yield peaks corresponding to the dominant periodicities, and this is shown in figure 22. Since the oxygen atoms are surrounded by aluminium atoms, the first peak in the transform gives the aluminium–oxygen distance. From the known mean bond length in α-alumina it is possible to determine the phase change and this turns out to be equivalent to a shift of 0.49 Å, which is close to the calculated value of 0.51 Å. The bond length in amorphous alumina can now be estimated, and the value obtained in this work was 1.89 Å, in good agreement with the results of conventional e.X.a.f.s. experiments with X-rays, which gave 1.90 Å.

PHILOSOPHICAL TRANSACTIONS OF THE ROYAL SOCIETY A MATHEMATICAL, PHYSICAL & ENGINEERING SCIENCES

PHILOSOPHICAL TRANSACTIONS OF THE ROYAL SOCIETY A MATHEMATICAL, PHYSICAL & ENGINEERING SCIENCES

Downloaded from rsta.royalsocietypublishing.org

PHILOSOPHICAL TRANSACTIONS OF THE ROYAL SOCIETY A MATHEMATICAL, PHYSICAL & ENGINEERING SCIENCES

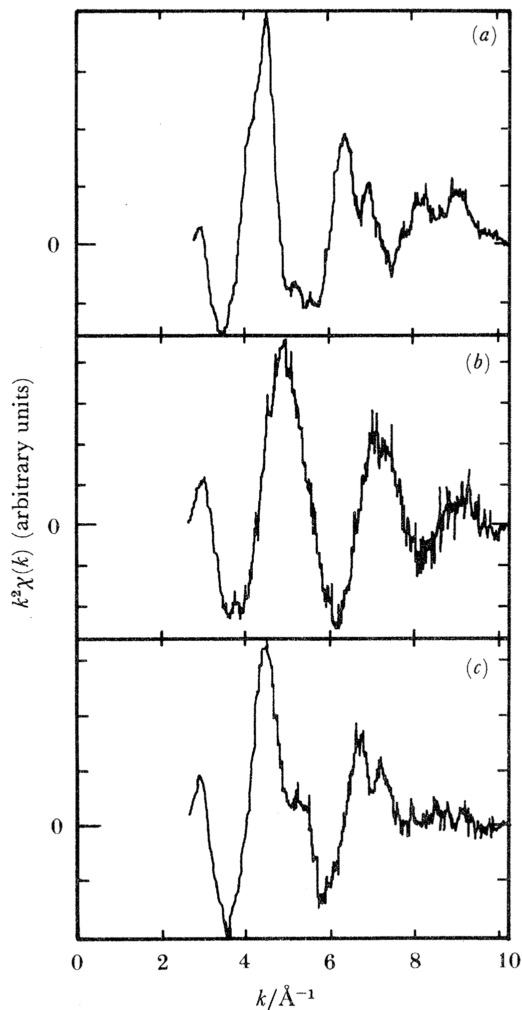

FIGURE 21. E.x.e.l.f.s. spectra from (*a*) α-alumina (*b*) amorphous alumina and (*c*) recrystallized amorphous alumina after background subtraction (Bourdillon *et al.* 1984).

PHILOSOPHICAL TRANSACTIONS OF THE ROYAL SOCIETY A MATHEMATICAL, PHYSICAL & ENGINEERING SCIENCES

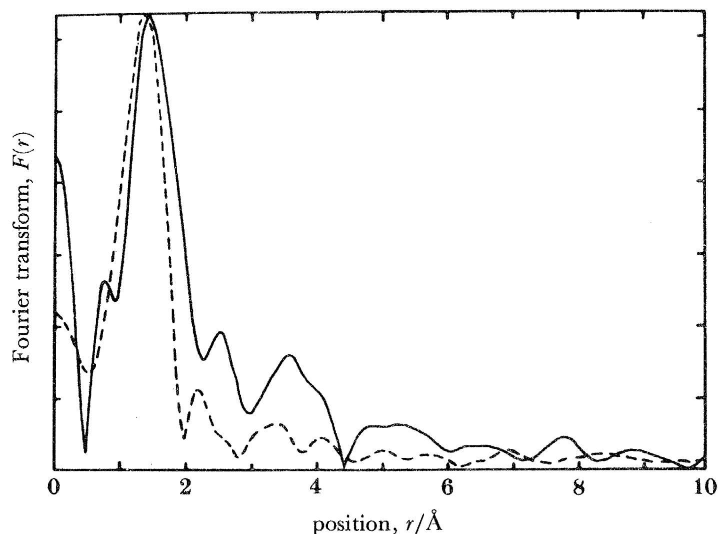

FIGURE 22. E.x.e.l.f.s. spectra shown in figure 21 after being Fourier transformed, but uncorrected for phase shift, for α-alumina (solid curve) and for the amorphous alumina (broken curve); the curves have been normalized to give the same first-shell peak height (Bourdillon, El Mashri & Forty 1984).

Downloaded from rsta.royalsocietypublishing.org

PHILOSOPHICAL TRANSACTIONS OF THE ROYAL SOCIETY A MATHEMATICAL, PHYSICAL & ENGINEERING SCIENCES

Although it is difficult to obtain e.x.e.l.f.s. data of the quality that one now expects to get almost routinely by using e.X.a.f.s., the great strength of e.x.e.l.f.s. lies in the fact that one can study truly microscopic regions as well as edges from light elements that are not readily accessible for study by e.X.a.f.s.

7. Compton scattering

All of the experiments described in the previous sections involve measuring the energy loss spectrum of the forward-scattering beam. However, if the beam is tilted and only those electrons that have been scattered through an angle of about 5° are made to enter the spectrometer, an entirely new feature is apparent (figure 23), and this is the electron equivalent of the Compton profile (Williams *et al.* 1983; Williams *et al.* 1984). To tie this in with other electron energy loss terminology, the Compton profile is a section through the Bethe surface at constant momentum transfer.

The Compton profile arises when both the energy and the momentum transfer are large. The electron that does the scattering is then ejected from its ground state into a plane-wave final state. Provided the energy transfer is sufficiently large, the impulse approximation is valid and the process may be treated as a collision between two free particles (see Williams & Thomas (1983) for a discussion of this approximation and cognate topics). We then solve the equations for the conservation of energy and momentum to obtain an expression for the energy transferred in the scattering process. If the electrons in the sample were stationary, this would depend only on the scattering angle. When the scattering angle is zero the energy transfer is zero and as the scattering angle increases the energy transfer increases. However, the electrons in the sample are not stationary, so that there will be an additional Doppler broadening of the energy distribution of the scattered radiation, as is clear from figure 23, which is the Compton profile. As always applies for Doppler effect, the broadening depends on only one component of the momentum, and this direction is defined by the scattering vector.

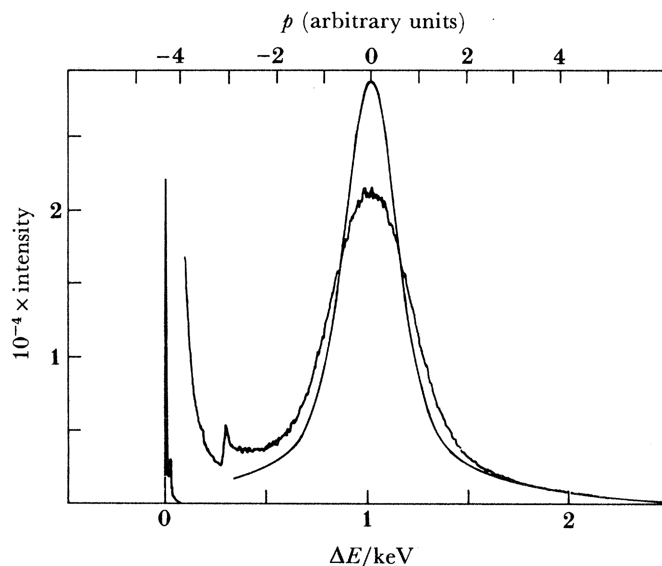

PHILOSOPHICAL TRANSACTIONS OF THE ROYAL SOCIETY A MATHEMATICAL, PHYSICAL & ENGINEERING SCIENCES

Figure 23. Experimental Compton profile of amorphous carbon measured using an electron microscope and theoretical Compton profile for a free atom of carbon (smooth line). The experimental data shows the zero-loss peak, the plasmon peak at about 25 eV and the carbon K edge at 284 eV.

Downloaded from rsta.royalsocietypublishing.org

To obtain theoretical Compton profiles, one starts from the position wavefunction $\psi(\boldsymbol{r})$. The momentum wavefunction $\chi(\boldsymbol{p})$ is then the Fourier transform of the position wavefunction

$$\chi(\boldsymbol{p}) = h^{-\frac{3}{2}} \iiint_{-\infty}^{+\infty} e^{-i\boldsymbol{p}\cdot\boldsymbol{r}/\hbar}\, \psi(\boldsymbol{r})\, d\boldsymbol{r}. \tag{7.1}$$

The momentum density $\rho(\boldsymbol{p})$ is the square modulus of the momentum wavefunction

$$\rho(\boldsymbol{p}) = \chi^*(\boldsymbol{p})\, \chi(\boldsymbol{p}) \tag{7.2}$$

and finally, the momentum density must be averaged over planes in momentum space so that the theoretical Compton profile is

$$J(p_z) = \iint_{-\infty}^{+\infty} \rho(p)\, dp_x\, dp_y. \tag{7.3}$$

With the aid of (7.1)–(7.3), the Compton profile provides a fairly direct measure of the ground state wavefunction of the electrons in the sample.

To illustrate the sensitivity of the Compton profile to changes in the wavefunction, the solid line (figure 23) is a theoretical Compton profile for a free atom of carbon, so that the differences between the two curves show the magnitude of the changes that take place when bonds are formed from the free-atom wavefunctions.

Since it is easier to think intuitively in position space than in momentum space, the analysis of Compton profile data is made easier if one Fourier transforms the profile to revert back to

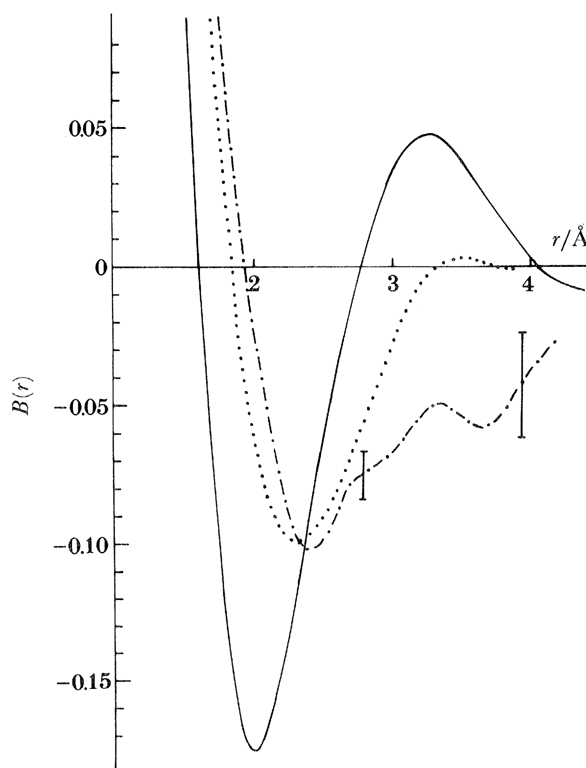

FIGURE 24. Fourier-transformed Compton profiles (reciprocal form factors) for diamond (solid line), graphite (dotted line) and amorphous carbon (chained line) showing that the bonding in amorphous carbon is predominantly graphitic.

Downloaded from rsta.royalsocietypublishing.org

position space. Now, the Fourier transform of the charge density is the form factor, so the Fourier transform of the momentum density has been dubbed the reciprocal form factor (r.f.f.). Since the Fourier transform of a product is the convolution of the Fourier transforms, the reciprocal form factor is nothing but the convolution of the position space wavefunction with itself.

Suppose then that we look at the Fourier-transformed Compton profiles of amorphous carbon, graphite and diamond shown in figure 24 (Williams *et al.* 1983). In all three cases there is a significant negative dip at a distance of about 2 Å. Now the r.f.f. is a self-convolution so that the negative dip reflects changes in the sign of the wavefunction and therefore the relative contributions of the s and p orbitals to each of the bonds. Indeed, we have been able to show (Williams *et al.* 1983) that the position of the dip depends primarily on the bond length and that the size of the dip reflects the hybridization state. In this particular example, Compton scattering shows clearly that the bonding in amorphous carbon is predominantly graphitic rather than adamantine. Note in particular that the film of carbon was so amorphous that we could not deduce its electronic structure from its diffraction pattern, yet, by probing the momentum density of the valence electrons we could, via Compton scattering, establish the nature of the bonding.

8. Multiple scattering

The great power of electron scattering derives from the strength of the electron–electron interaction and it is this that makes it possible to study matter on a truly atomic scale. However, this also means that multiple scattering events will make a significant, sometimes overwhelming, contribution to the observed scattering unless the samples are very thin indeed. Frequently it is not possible to obtain samples for which the multiple scattering contribution is sufficiently small and it is then necessary to allow for these effects. In lattice image calculations this problem is well known and understood (Goodman & Moodie 1974). However, it is also important to allow for the multiple scattering in e.e.l.s. studies.

Except for Compton scattering this is not difficult. The dominant inelastic process is plasmon scattering in the forward direction, and as we have already seen one can easily obtain four or five distinct plasmon peaks, each corresponding to successively more multiple scattering events. The deconvolution procedure is then straightforward, especially if one makes use of the fact that the distribution of the various orders of multiple scattering follows a Poisson distribution (Johnson & Spence 1974). In this case one can simply Fourier transform the data, take the logarithm of the Fourier transform and then transform back again. As an illustration, one of the plasmon spectra of silicon shown in figure 3 has been deconvoluted and all of the plasmon lines except the first are effectively removed (figure 25). As a further illustration we have deconvoluted a measurement of the e.e.l.s. spectrum of boron nitride (figure 26). Again it is clear that the deconvolution procedure works well (see Egerton *et al.* 1985 for further details).

Unfortunately, for electron Compton scattering the situation is entirely different. Whereas all of the other energy loss processes are measured in the forward direction, where they are most intense, and, in addition they do not depend strongly on the scattering angle, the Compton profile is measured at high angles and the peak shift and the width of the Compton profile depend critically on the scattering angle. As a result, the dominant multiple-scattering events in the Compton profile arise from double-scattering events in which a Bragg scattering produces the high angle and a Compton scattering the energy loss.

PHILOSOPHICAL TRANSACTIONS OF THE ROYAL SOCIETY A MATHEMATICAL, PHYSICAL & ENGINEERING SCIENCES

PHILOSOPHICAL TRANSACTIONS OF THE ROYAL SOCIETY A MATHEMATICAL, PHYSICAL & ENGINEERING SCIENCES

Downloaded from rsta.royalsocietypublishing.org

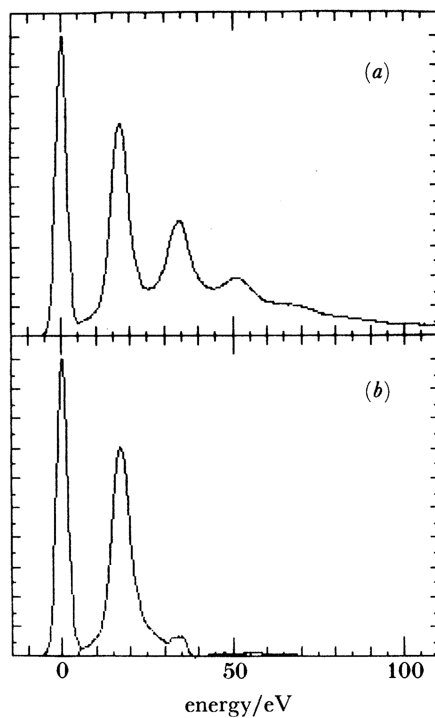

FIGURE 25. Plasmon spectrum of silicon taken from the third thickness fringe in figure 10: (*a*) before and (*b*) after deconvolution.

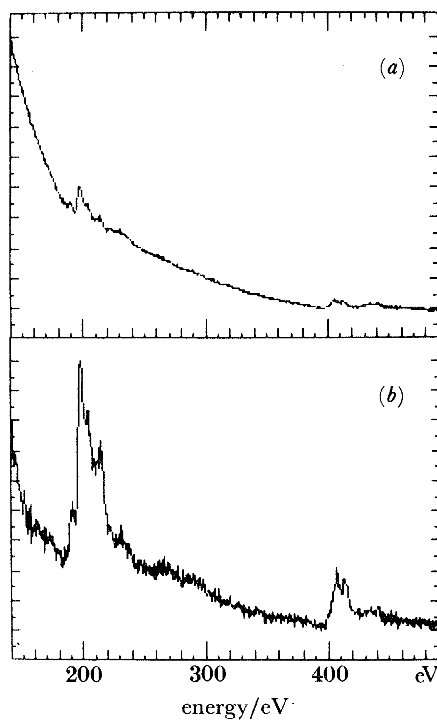

FIGURE 26. E.e.l.s. spectrum of boron nitride, showing the boron edge at 188 eV and the nitrogen edge at 402 eV; (*a*) before and (*b*) after deconvolution.

PHILOSOPHICAL TRANSACTIONS OF THE ROYAL SOCIETY A MATHEMATICAL, PHYSICAL & ENGINEERING SCIENCES

PHILOSOPHICAL TRANSACTIONS OF THE ROYAL SOCIETY A MATHEMATICAL, PHYSICAL & ENGINEERING SCIENCES

Downloaded from rsta.royalsocietypublishing.org

To account for the multiple scattering, in the lowest order of approximation, each Bragg beam can be treated as a source of Compton scattering, bearing in mind that having set the aperture at some angle to the incident beam direction, each Bragg beam will make its own angle with the aperture. But simply to calculate the intensity in each of the Bragg beams requires a full dynamical scattering simulation of the experiment. Fortunately, programs for doing this have been developed for lattice image calculations and we have been able to adapt these to the calculation of multiple scattering in electron Compton scattering.

To illustrate the magnitude of the problem, figure 27 shows the result of simulating a Compton scattering experiment from silicon. We have assumed an incident beam energy of 100 keV, and the incident beam enters the sample in the direction of the (100) zone axis. This solid line is the contribution from the (000) beam, which is effectively the single scattering. However, in addition to this, contributions must be included from all of the other beams in the diffraction pattern. Even for a 5 Å layer of silicon atoms there is some multiple scattering, as can be seen from the broken line in figure 27*a*, which gives the total scattering. For a sample of silicon 1000 Å thick, the situation is considerably worse and the multiple scattering completely dominates the single scattering (figure 27*b*). However, from simulations of the multiple scattering and by studying the way in which it varies with the incident beam energy, crystal orientation, sample thickness and the atomic number of the elements in the sample, it should be possible to choose conditions under which is it not too severe and perhaps allow for it in our measurements.

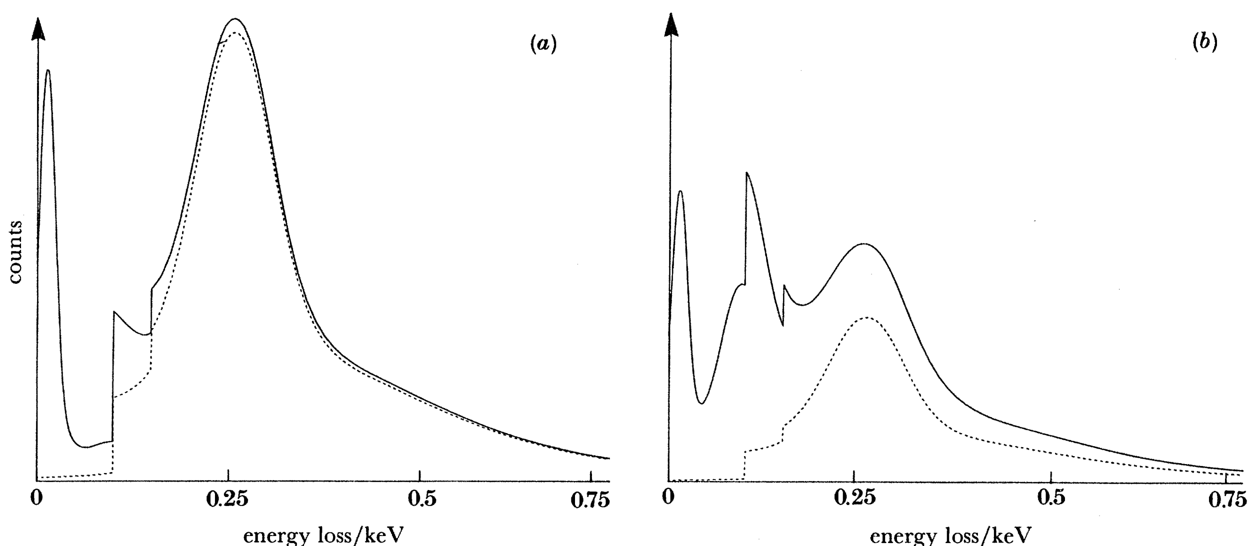

FIGURE 27. Calculated Compton profiles for silicon: (*a*) for a 5 Å thick slice and (*b*) for a 1000 Å thick slice. The electron beam enters in the (100) direction. The broken line gives the single scattering and the solid line the total, including Bragg–Compton double-scattering events.

9. Conclusions

Much of the work described here deals with very thin samples and not with surfaces *per se*. But by using appropriate techniques (Colliex *et al.* 1985), a substantial part of what we have discussed can be adapted to an exclusive surface study. This may well be achieved by using

Downloaded from rsta.royalsocietypublishing.org

an instrument such as the Vacuum Generators HB 501 STEM, which has a good vacuum, of the order of 10^{-10} Torr (*ca.* 13 nPa) facilities for cleaning and preparing specimens. It is also fitted with an Auger spectrometer. One can then either look at small particles and skim the surface with a fine probe, or use bulk specimens, in which case the sample must be turned on its edge and the measurements done at a glancing angle.

In summary, the electron microscope combined with an electron energy loss spectrometer affords a convenient means of investigating numerous physical and chemical properties of matter. A great asset is that with one and the same sample one can record images and diffraction patterns, cathodo-luminescence, X-ray and Auger spectra, as well as the e.e.l.s. spectra described here. Few techniques can rival this as a means of extracting, from minute samples, information about oxidation states, structure and bonding and as a tool for phase identification and characterization.

We thank the S.E.R.C., the Royal Society and the University of Cambridge for financial support, and Dr D. Imeson for measuring the spectrum shown in figure 7.

References

Berger, S. D. & Pennycook, S. J. 1982 *Nature, Lond.* **298**, 635.
Bohm, D. & Gross, E. P. 1949*a* *Phys. Rev.* **75**, 1851–1864.
Bohm, D. & Gross, E. P. 1949*b* *Phys. Rev.* **75**, 1864–1876.
Bohm, D. & Pines, D. 1951 *Phys. Rev.* **82**, 625.
Bohm, D. & Pines, D. 1953 *Phys. Rev.* **92**, 609–625.
Bourdillon, A. J., El Mashri, S. M. & Forty, A. J. 1984 *Phil. Mag.* A **49**, 341–352.
Bursill, L. A., Egerton, R. F., Thomas, J. M. & Pennycook, S. J. 1981 *J. chem. Soc. Faraday Trans.* II **77**, 1367–1373.
Colliex, C., Manoubi, T., Gasgnier, M. & Brown, L. M. 1985 (In preparation).
Egerton, R. F. 1978 *Ultramicroscopy* **3**, 243–251.
Egerton, R. F. 1979 *Ultramicroscopy* **4**, 169–179.
Egerton, R. F. 1981*a* *Ultramicroscopy* **6**, 297–300.
Egerton, R. F. 1981*b* *Ultramicroscopy* **7**, 207–210.
Egerton, R. F. 1981*c* *J. Microsc.* **123**, 333–337.
Egerton, R. F. 1982 *Phil. Trans. R. Soc. Lond.* A **305**, 521.
Egerton, R. F., Williams, B. G. & Sparrow, T. G. 1985 *Proc. R. Soc. Lond.* A **398**, 395–404.
Evans, T. & Phaal, C. 1962 *Proc. R. Soc. Lond.* A **270**, 535–552.
Goodman, P. & Moodie, A. F. 1974 *Acta crystallogr.* A **30**, 280.
Jefferson, D. A., Millward, G. R. & Thomas, J. M. 1976 *Acta crystallogr.* A **32**, 823.
Jefferson, D. A., Thomas, J. M., Uppal, M. K. & Grasselli, R. K. 1983 *Chem. Commun.*, p. 594.
Johnson, D. W. & Spence, J. C. H. 1974 *J. Phys.* D **7**, 771–780.
Jones, W., Sparrow, T. G., Williams, B. G. & Herley, P. J. 1984 *Mater. Lett.* **2**, 377–379.
Kramers, H. A. 1947 *Physica* **13**, 401.
Krane, K. J. & Raether, H. 1976 *Phys. Rev. Lett.* **37**, 1355–1357.
Kronig, R. 1949 *Physica* **14**, 667.
Kronig, R. & Korringa, J. 1943 *Physica* **10**, 406.
Lang, W. 1948 *Optik* **3**, 233.
Pines, D. 1953 *Phys. Rev.* **92**, 626–636.
Pines, D. & Bohm, D. 1952 *Phys. Rev.* **85**, 338.
Raether, H. 1980 Excitation of plasmons and interband transitions by electrons. *Springer Tracts in Modern Physics*, vol. 88. Berlin: Springer Verlag.
Rao, C. N. R., Sparrow, T. G., Williams, B. G. & Thomas, J. M. 1984 *Chem. Commun.* pp. 1238–1240.
Ruthemann, G. 1948 *Ann. Phys.* **2**, 113.
Sparrow, T. G., Williams, B. G., Rao, C. N. R. & Thomas, J. M. 1984 *Chem. Phys. Lett.* **108**, 547–550.
Sparrow, T. G., Williams, B. G., Thomas, J. M., Jones, W., Herley, P. J. & Jefferson, D. A. 1983 *Chem. Commun.*, p. 1432.
Stephens, A. P. & Brown, L. M. 1981 EXELFS in graphitic boron nitride. In *Quantitative microanalysis with high spatial resolution*, pp. 152–158. London: The Metals Society.
Thomas, J. M. 1982 *Ultramicroscopy* **8**, 13.

Downloaded from rsta.royalsocietypublishing.org

MATHEMATICAL, PHYSICAL & ENGINEERING SCIENCES
PHILOSOPHICAL TRANSACTIONS OF THE ROYAL SOCIETY A

Thomas, J. M. 1983 In *Inorganic chemistry towards the 21st century* (ed. M. H. Chisholm). *ACS Publ.* no. 211, p. 445.
Thomas, J. M., Rao, C. N. R., Williams, B. G. & Sparrow, T. G. 1984 *J. phys. Chem.* **88**, 5770–5772.
Tonks, L. & Langmuir, I. 1929 *Phys. Rev.* **33**, 195.
Vasudevan, S., Rayment, T., Williams, B. G. & Holt, R. 1984 *Proc. R. Soc. Lond.* A **391**, 109–124.
Weinberg, W. H. 1978 *A. Rev. phys. Chem.* **29**, 115.
Williams, B. G. (ed.) 1977 *Compton scattering – the investigation of electron momentum densities*. New York: McGraw-Hill.
Williams, B. G., Sparrow, T. G. & Egerton, R. F. 1984 *Proc. R. Soc. Lond.* A **393**, 409–422.
Williams, B. G., Sparrow, T. G. & Thomas, J. M. 1983 *Chem. Commun.*, p. 1434.
Williams, B. G. & Thomas, J. M. 1983 *Int. Rev. phys. Chem.* **3**, 39–82.
Williams, B. G., Vasudevan, S. & Rayment, T. 1983 *Proc. R. Soc. Lond.* A **388**, 219–228.

Discussion

D. Norman (*S.E.R.C., Daresbury Laboratory, Warrington, U.K.*). Dr Williams stated that e.x.e.l.f.s. can be used to study the first-row elements whereas e.X.a.f.s. cannot, given as his example measurements of the oxygen K-edge in alumina. In fact, e.X.a.f.s. experiments on this very system have been made (Norman *et al.* 1981), in conjunction with surface studies of the progressive oxidation of aluminium, in which it was shown that one could deduce the relative proportions of $Al–O_4$ to $Al–O_6$ local units in amorphous aluminas of different forms. Some e.X.a.f.s. studies above the C, N, O and F K-absorption edges have been reviewed in Stöhr *et al.* (1980).

References

Norman, D., Brennan, S., Jaeger, R. & Stöhr, 1981 *Surf. Sci.* **105**, 297–306.
Stöhr, J., Jaeger, R., Feldhaus, J., Brennan, S., Norman, D. & Apai, G. 1980 *Appl. Opt.* **19**, 3911–3919.

J. M. Thomas. The remarks made during our presentation about the difficulties of carrying out e.X.a.f.s. studies on the light elements were not intended to suggest that these were impossible. Denely *et al.* (1980) and Stöhr *et al.* (1985) each showed in the late 1970s that, by recording the intensity of the secondary electrons emitted as a consequence of K-shell absorption, some useful structural information about the environment of carbon atoms at solid surfaces could be obtained. The papers quoted by Dr Norman constitute a logical extension of that earlier approach and he is right to draw attention to them. Of late, however, thanks to improvements in recording the fluorescence emission consequent upon X-ray absorption by light elements, more revealing data have emerged about the environment and bonding of light elements attached to solid surfaces. Stöhr, for example (Stöhr *et al.* 1985), has established that methoxy groups (CH_3O) bond to Cu(100) surface end-downwards in a fourfold hollow site, with a Cu–O distance of 1.97 Å.

What we wanted to emphasize in our paper was that the question of tackling the environment of light elements in microcrystalline solids (consisting of numerous phases) is more accessible experimentally by using electron microscopes fitted with electron spectrometers than by using conventional synchrotron sources. One has to concede, however, that extraction of reliable bond distances via the e.x.e.l.f.s. route is more arduous theoretically than via the e.X.a.f.s. route, especially now that Stöhr *et al.* have produced correlation between bond distances and frequencies of photon emission.

References

Denely, D., Perfetti, P., Williams, R. S. & Shirley, D. A. 1980 *Phys. Rev.* B **21**, 2267–2273.
Stöhr, J., Outka, D. A., Madix, R. J. & Döbler, U. 1985 *Phys. Rev. Lett.* **12**, 1256.

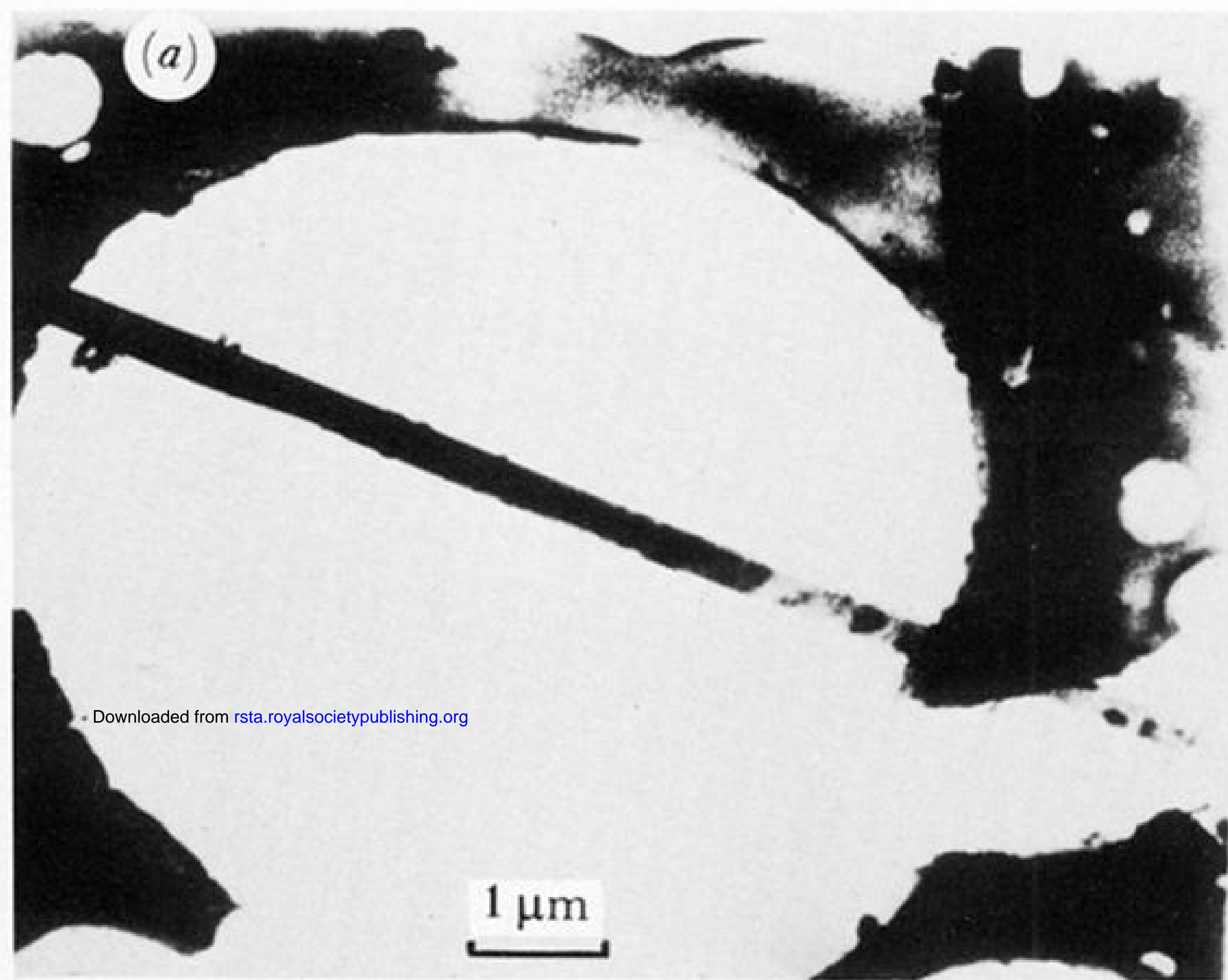

Downloaded from rsta.royalsocietypublishing.org

MATHEMATICAL, PHYSICAL & ENGINEERING SCIENCES
PHILOSOPHICAL TRANSACTIONS OF THE ROYAL SOCIETY A

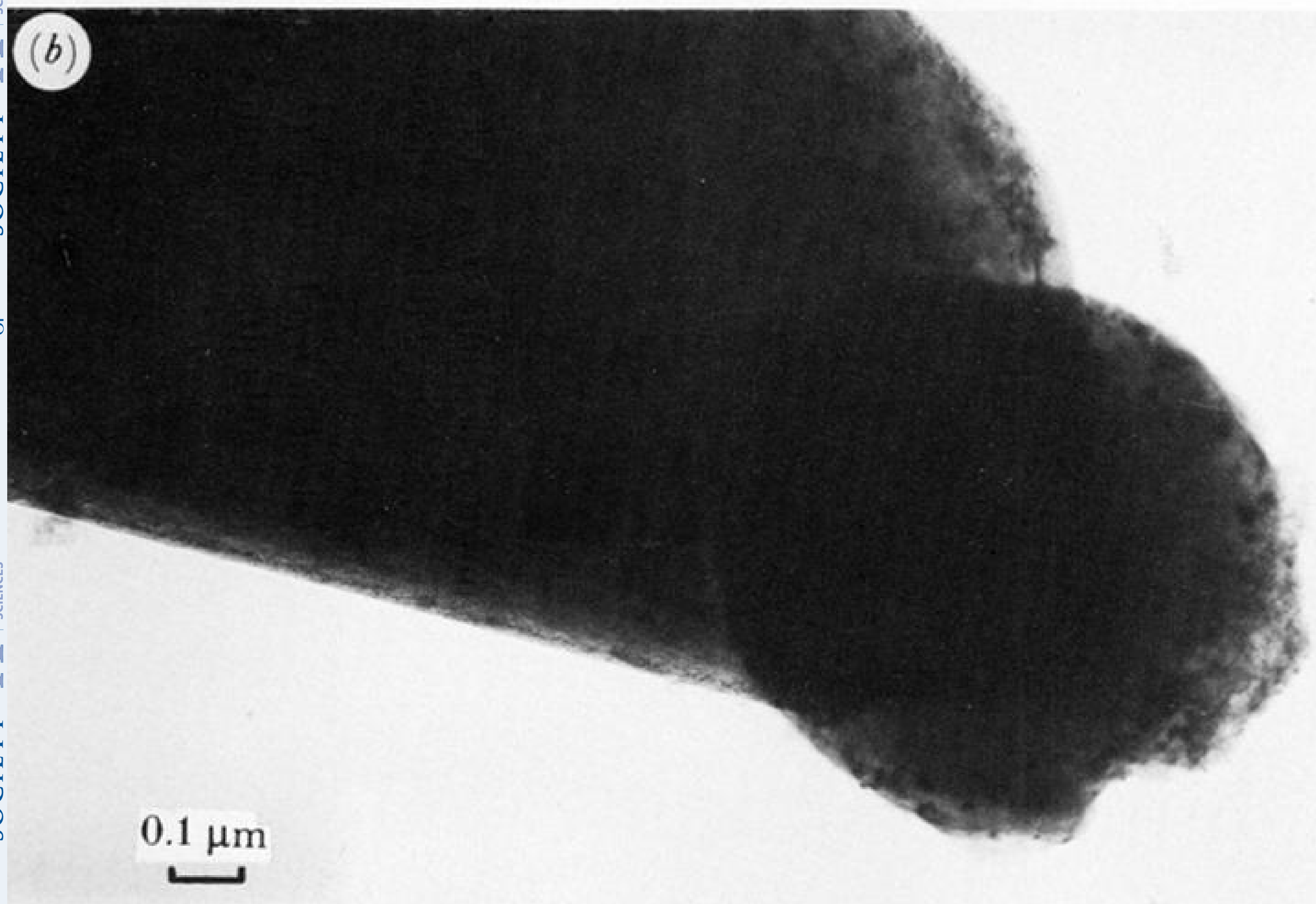

MATHEMATICAL, PHYSICAL & ENGINEERING SCIENCES
PHILOSOPHICAL TRANSACTIONS OF THE ROYAL SOCIETY A

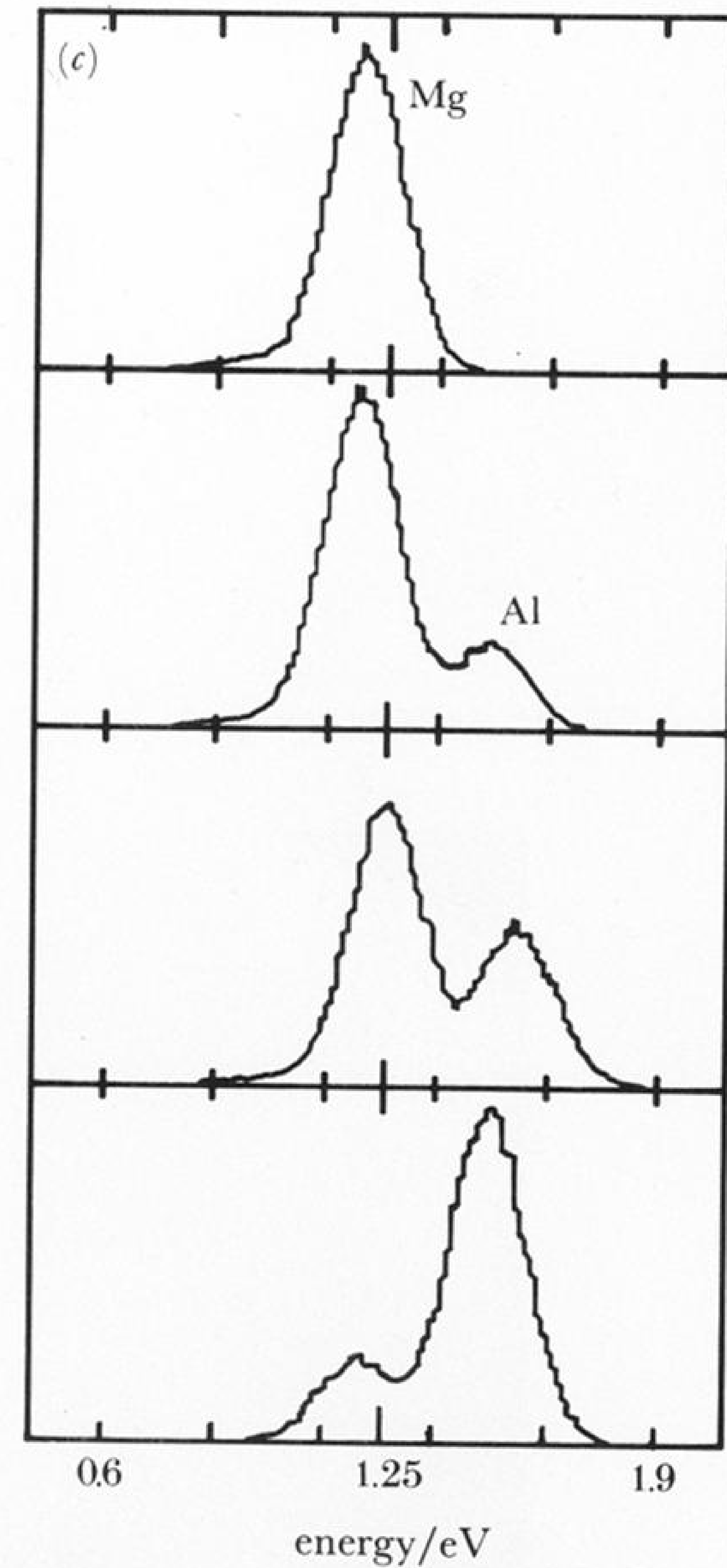

FIGURE 5. (a) Magnesium whisker on holey carbon film. (b) Tip of whisker where aluminium is present. (c) E.d.a.X. spectra of whisker from regions progressively closer to tip.

PHILOSOPHICAL TRANSACTIONS OF THE ROYAL SOCIETY A MATHEMATICAL, PHYSICAL & ENGINEERING SCIENCES

PHILOSOPHICAL TRANSACTIONS OF THE ROYAL SOCIETY A MATHEMATICAL, PHYSICAL & ENGINEERING SCIENCES

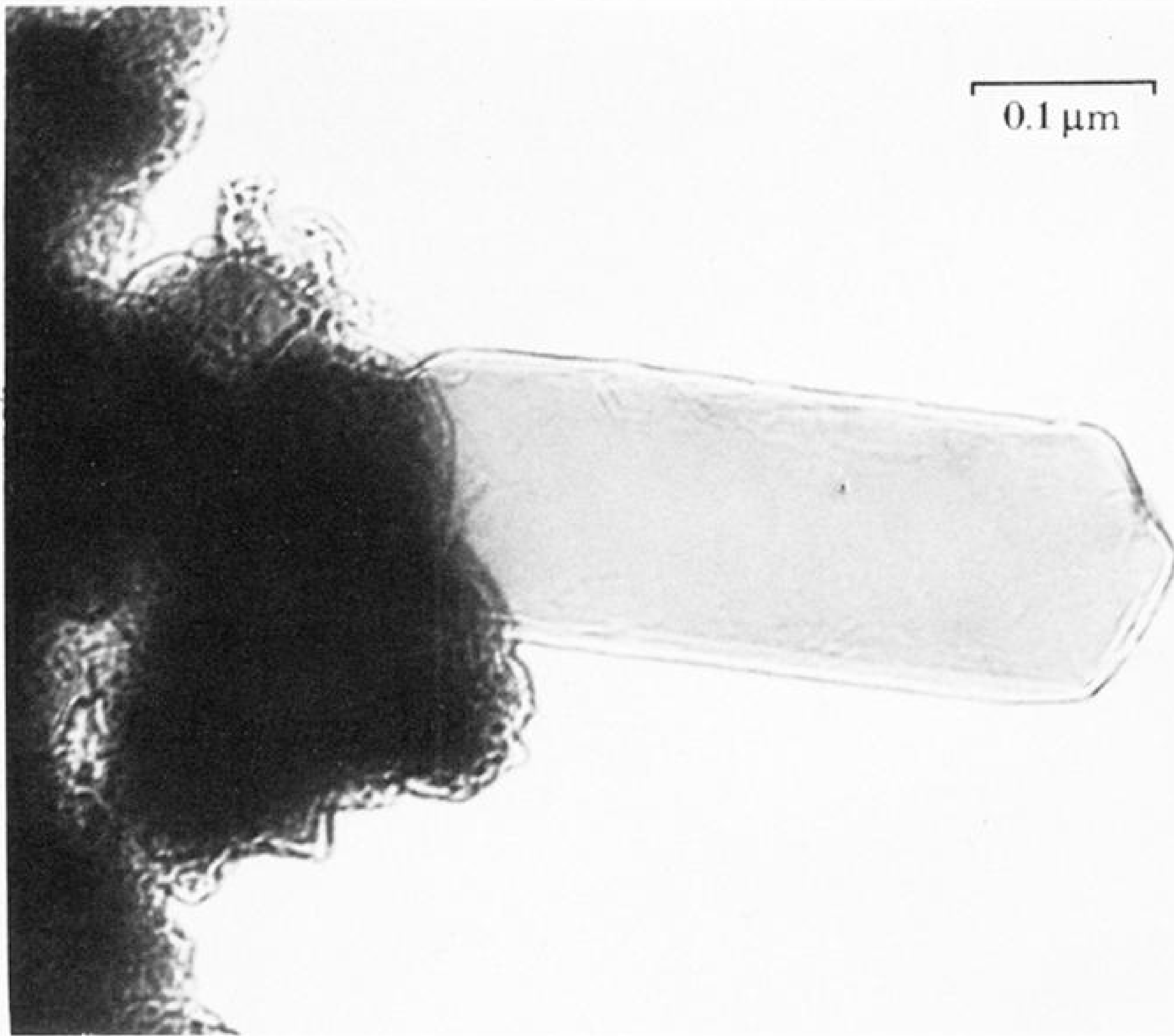

FIGURE 8. Sodium crystal grown out from $NaAlH_4$ sample, as a result of exposure to the electron beam.

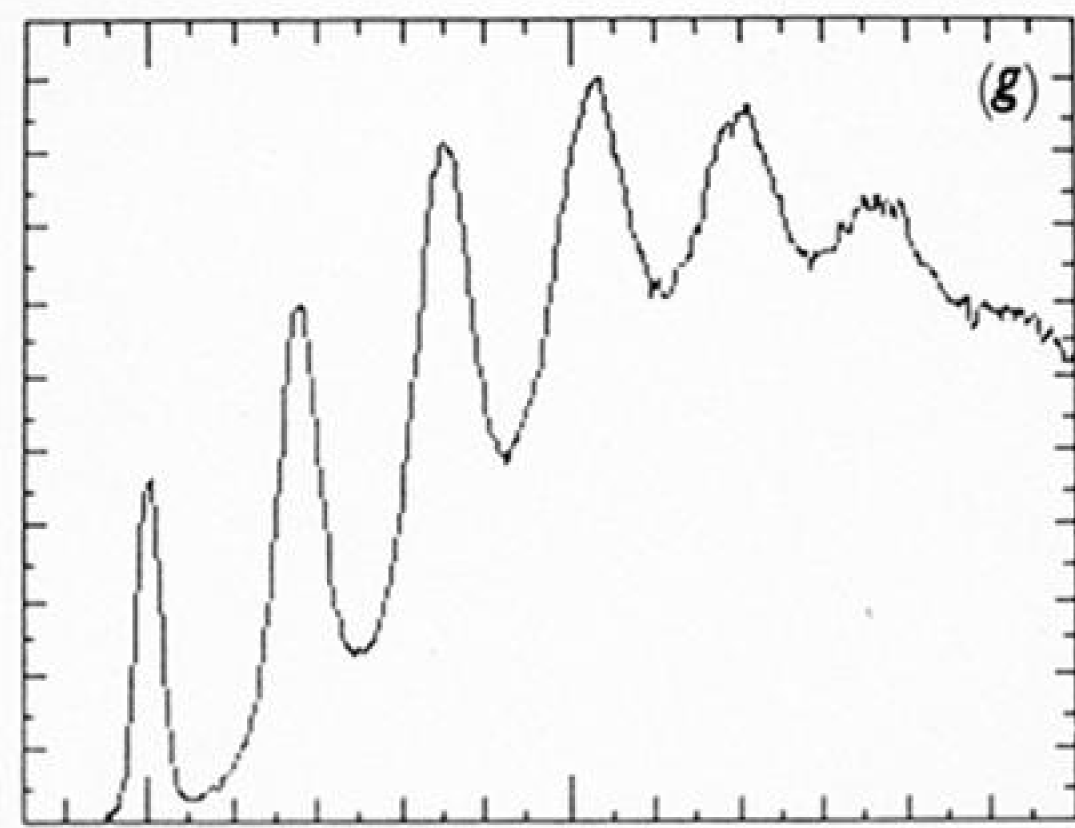

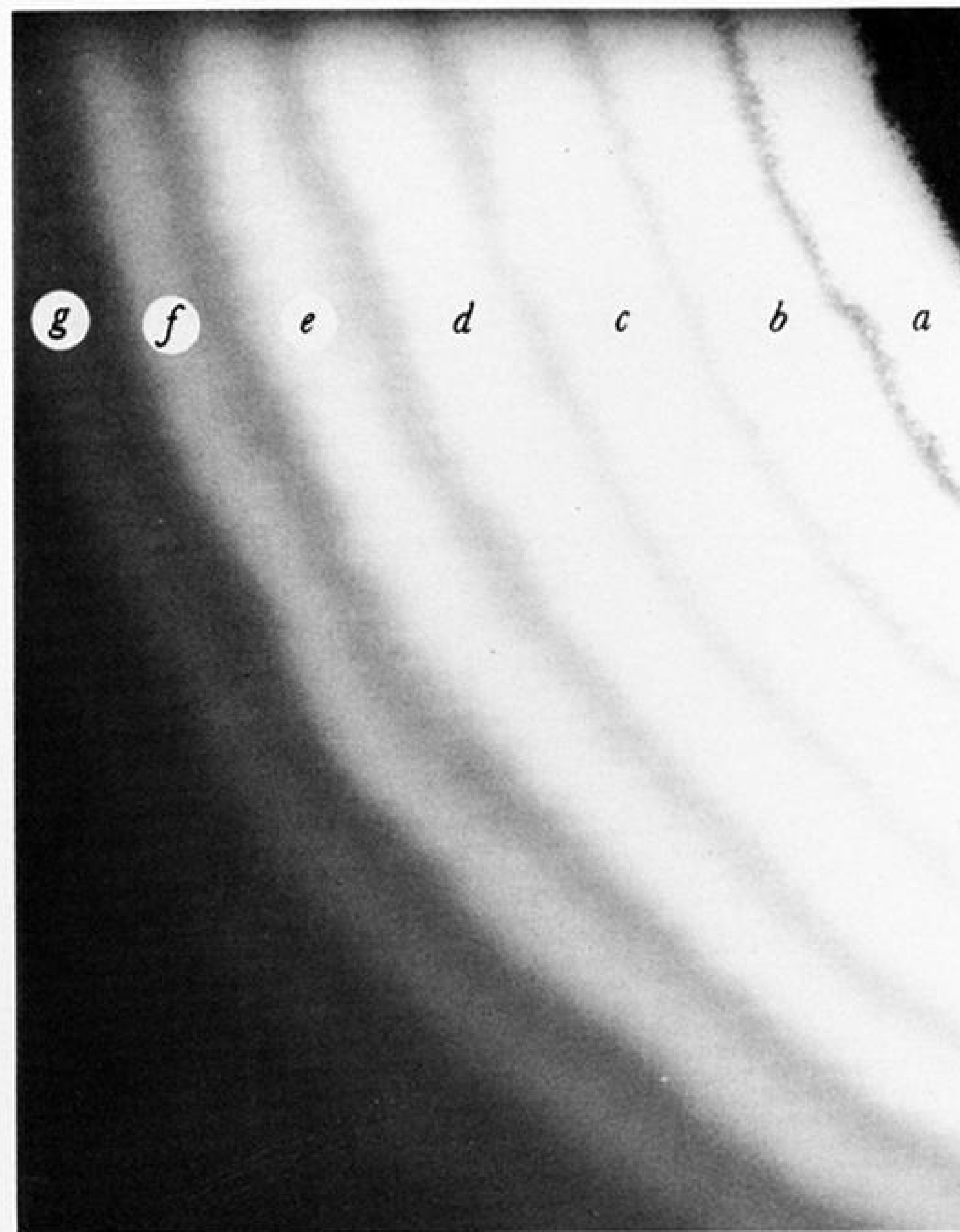

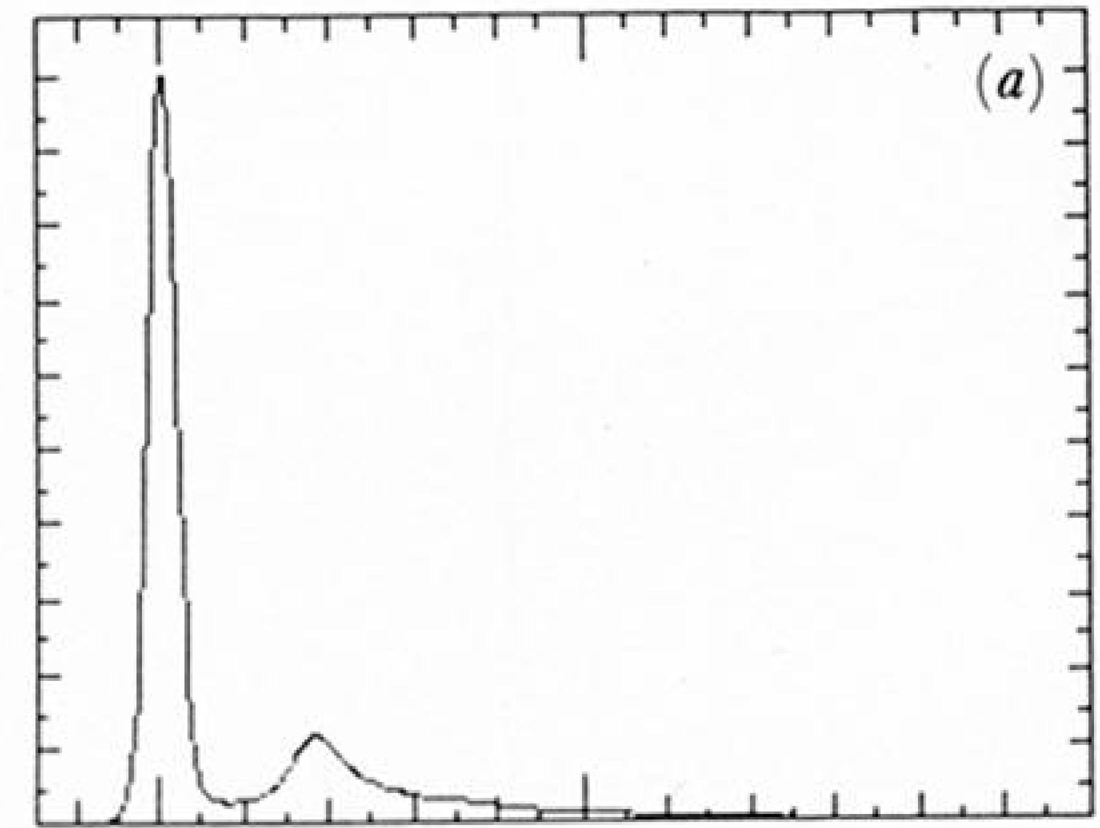

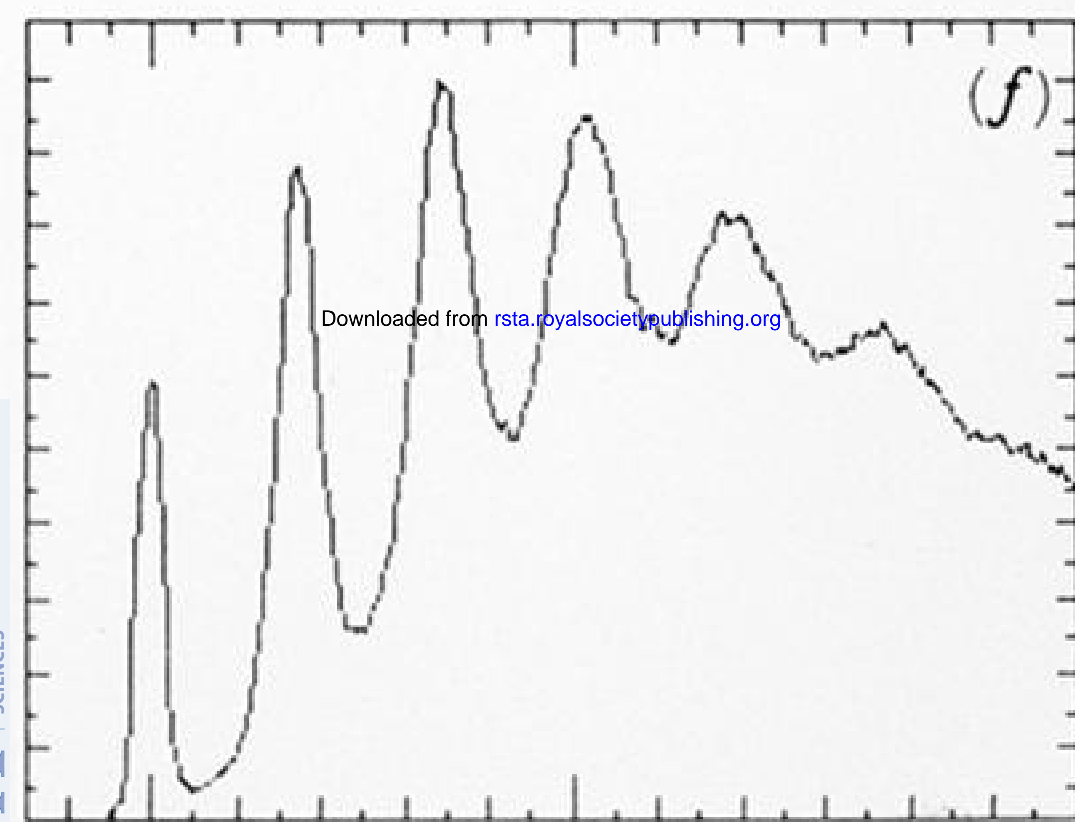

Downloaded from rsta.royalsocietypublishing.org

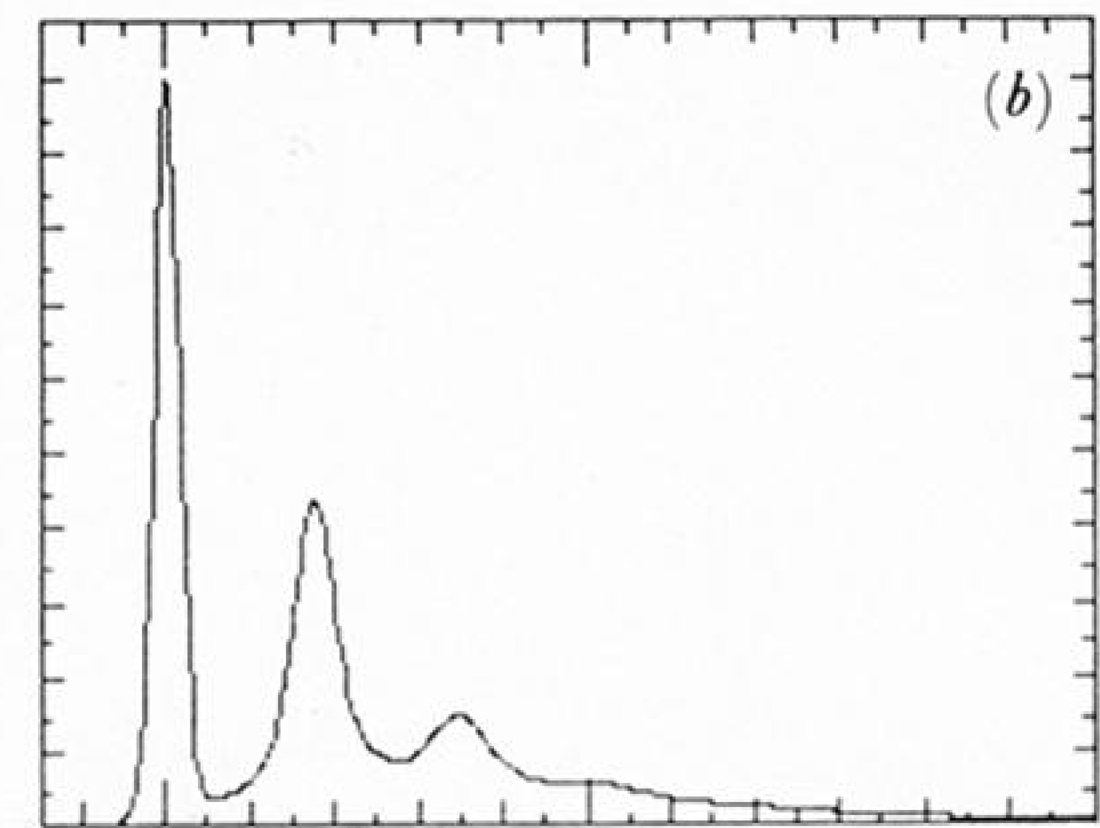

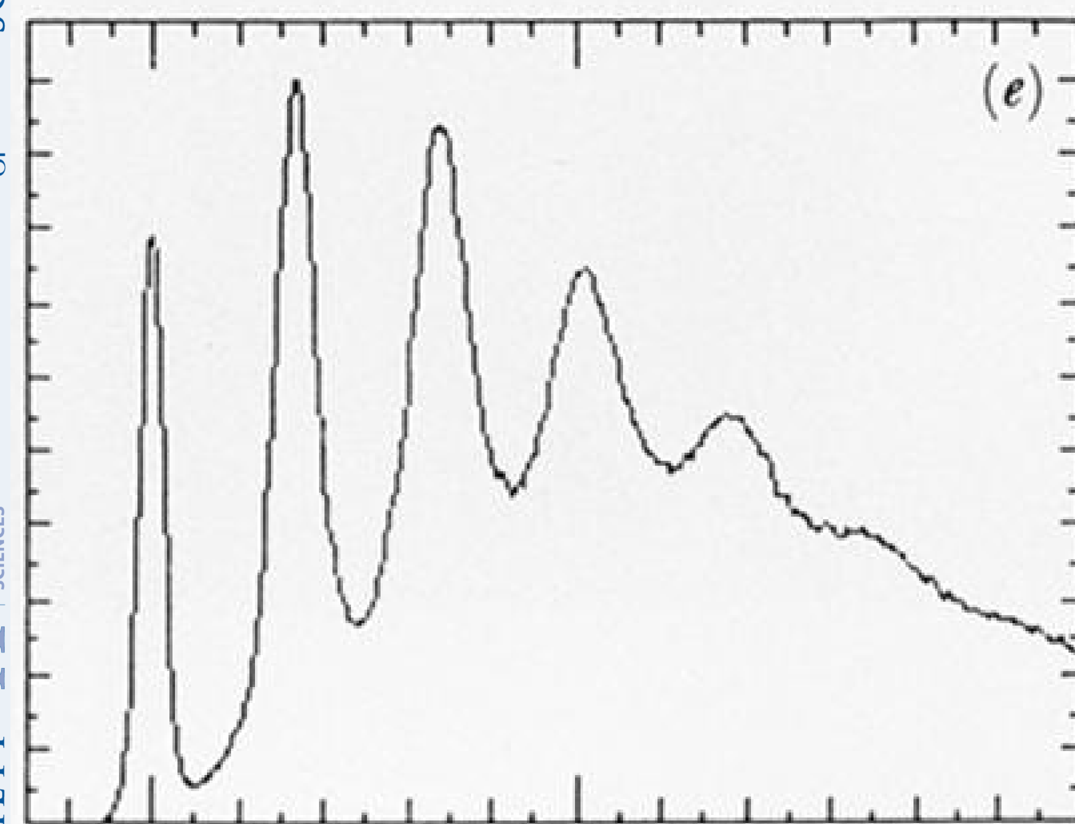

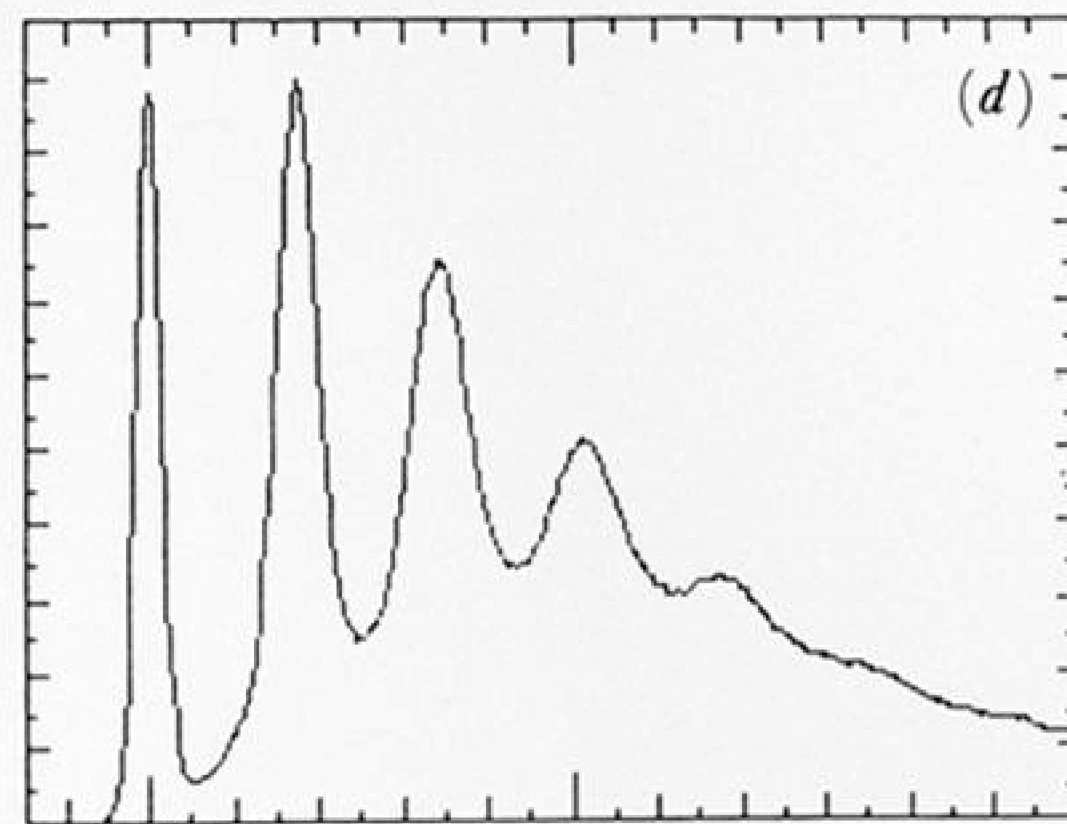

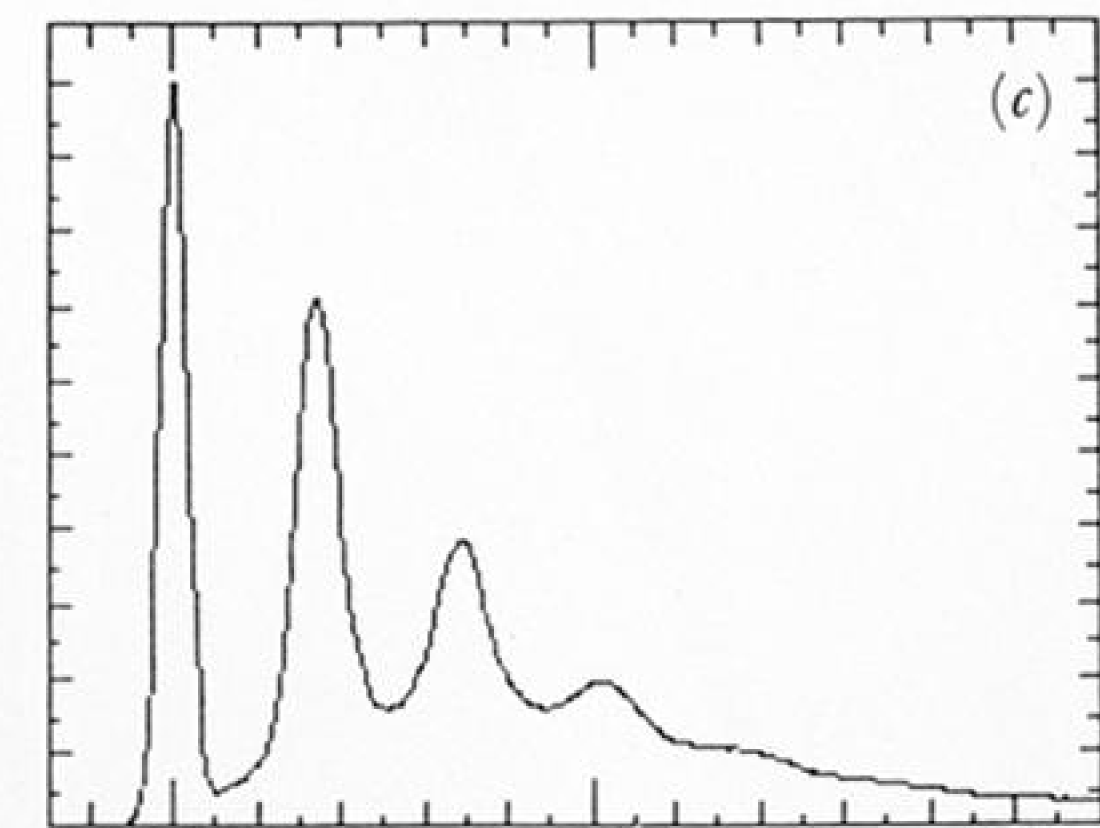

FIGURE 10. Thickness fringes in a single crystal of silicon. There is a hole at the top right corner and the thickness increases towards the bottom left. Plasmon spectra measured at each successive fringe as indicated. Each fringe corresponds to an increase in thickness of about 600 Å.

PHILOSOPHICAL TRANSACTIONS OF THE ROYAL SOCIETY A MATHEMATICAL, PHYSICAL & ENGINEERING SCIENCES

PHILOSOPHICAL TRANSACTIONS OF THE ROYAL SOCIETY A MATHEMATICAL, PHYSICAL & ENGINEERING SCIENCES

PHILOSOPHICAL TRANSACTIONS OF THE ROYAL SOCIETY

MATHEMATICAL, PHYSICAL & ENGINEERING SCIENCES
THE ROYAL SOCIETY A
PHILOSOPHICAL TRANSACTIONS OF

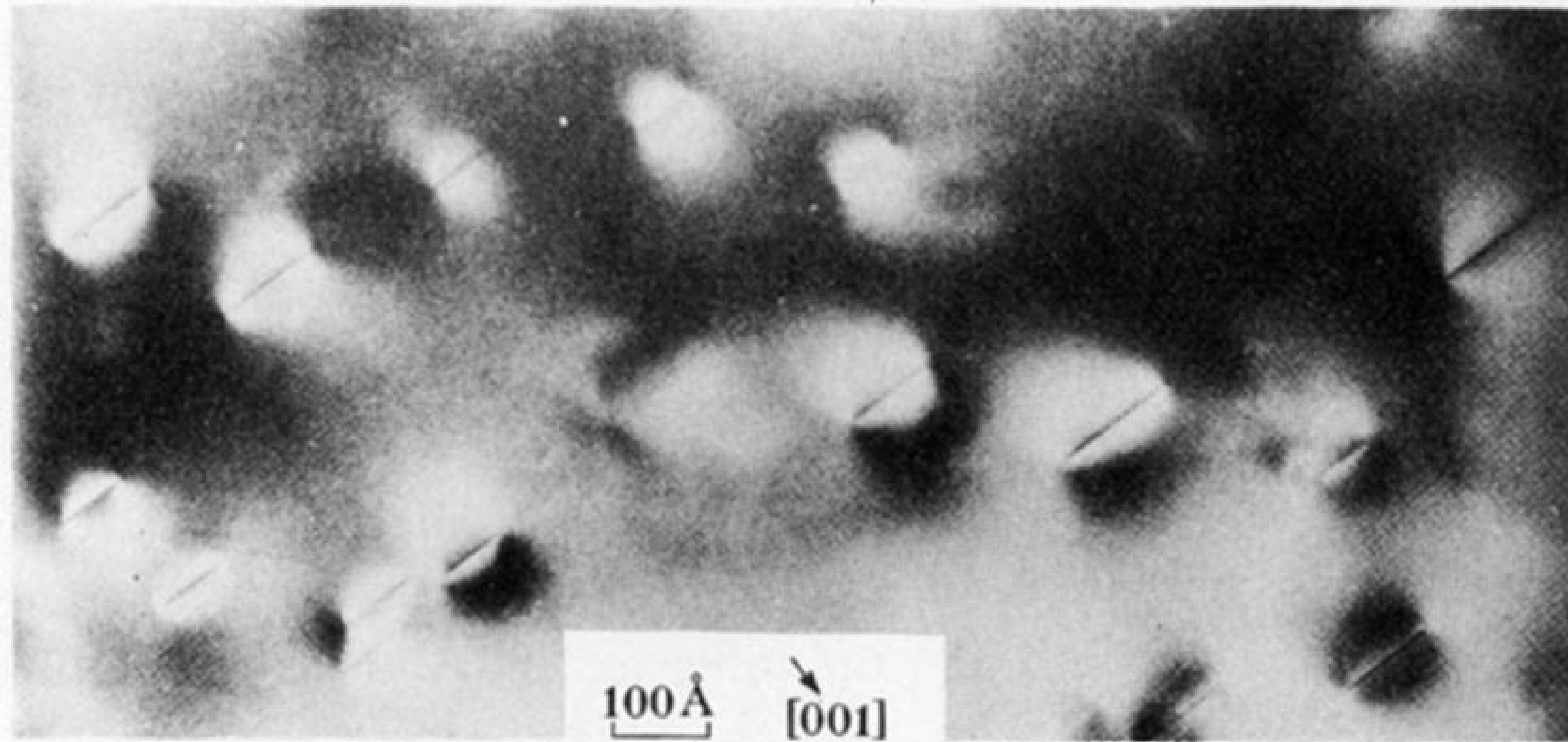

FIGURE 14. Electron micrograph showing small (100–200 Å diameter) (001) platelets in [100] projection of type 1A diamond. Dark lines indicate edge-on platelets, which are surrounded by black and white strain contrast (Bursill *et al.* 1981). (1 Å = 10^{-1} nm = 10^{-10} m.)